Alma Mater Studiorum – University of Bologna

SCHOOL OF SCIENCE
Department of Industrial Chemistry "Toso Montanari"

Second cycle degree in

Low Carbon Technologies and Sustainable Chemistry

LM-71 – Industrial Chemistry

Synthesis and characterization of high-nuclearity Rh-Au clusters stabilized by carbonyl ligands

Experimental degree thesis

CANDIDATE

Andrea Masetti

SUPERVISOR

Prof. Cristina Femoni

CO-SUPERVISOR

Guido Bussoli

Academic Year 2020-2021

ABSTRACT

The aim of this project was to synthesize and characterize new high nuclearity heterometallic Rh-Au clusters. The reactivity of rhodium clusters was studied starting from the precursor $[Rh_7(CO)_{16}]^{3-}$, which was oxidated with different Au^{3+} and Au^{+} salts. Its behaviour was analysed in different reaction conditions, changing each time the Rh:Au stoichiometric ratio and solvents, under controlled CO atmosphere. Multiple new clusters were obtained: $[Rh_{10}Au(CO)_{26}]^{3-}$, $[Rh_{16}Au_6(CO)_{36}]^{4-}$, $[Rh_{19}Au_5(CO)_{40}]^{4-}$ and $[Rh_{20}Au_7(CO)_{45}]^{5-}$. A clean and reproducible synthetic pathway to synthesize the new $[Rh_{10}Au(CO)_{26}]^{3-}$ was discovered. Moreover, a new synthetic pathway to synthetize $[Rh_{16}Au_6(CO)_{36}]^{6-}$ was discovered. Each compound has been characterized via FT-IR spectroscopy and single crystal X-ray diffractometry; $[Rh_{10}Au(CO)_{26}]^{3-}$, $[Rh_{16}Au_6(CO)_{36}]^{4-}$ and $[Rh_{16}Au_6(CO)_{36}]^{6-}$ have been also analysed via ESI-MS analysis. Finally, chemical reactivity tests on $[Rh_{10}Au(CO)_{26}]^{3-}$ were conducted, verifying that a consecutive pathway starting from the latter leads to the formation of $[Rh_{16}Au_6(CO)_{36}]^{4-}$.

INDEX

1. INTRODUCTION

Metal carbonyl clusters are compounds, or molecular ions, containing two or more metal atoms linked, in part or completely, by metal-metal bonds [1] and containing an external carbon dioxide shell which stabilizes the central structure [2] while avoiding its coalescence.

A large number of molecules are able to stabilize these compounds but, among them, carbon monoxide has a central role since it is able to stabilize the relatively low oxidation state of the metal centre, which usually also ranges to negative values. As a matter of fact, CO can donate an electron pair to the empty orbitals of the metal atom through a σ donation, acting as a Lewis base, while also accepting electron density from the metal on its empty antibonding orbitals through π backdonation, therefore also acting as a Lewis acid. It is the synergism among the σ donation and the π backdonation that causes the carbon monoxide to be a strong field ligand, thus motivating its presence at the end of the spectrochemical series. Moreover, CO is a narrow ligand with limited steric hindrance, hence it can coordinate to the metal in multiple fashions: terminal, edge-bridging, or face-bridging position.

The number of ligands that coordinate to the metal centre is not random: the total of the metal atoms' valence electrons are added to the ones provided by the ligands and the possible negative charges in order to attain the CVE (Cluster Valence Electrons), which fill the CVMO (Cluster Valence Molecular Orbitals) of the compound. Most frequently, clusters that have the same metal skeletal geometry abide by the electronic counting rules so as to achieve the same CVE value, regardless of the type of metal, the number of ligands or the overall charge of the cluster. [3] [4] However, some high-nuclearity clusters (structures containing more than 10-12 metal atoms) are known not to always abide by these rules. [5]

This behaviour depends on various factors, the main one being the gradual loss of the HOMO-LUMO gap as the nuclearity of the cluster increases. This happens as a

result of the number of metal-metal interactions that exceed the number of metal-CO ones when the ratio between the metal atoms on the centre and on the surface of the structure increases. For instance, it has been empirically verified that in clusters with nuclearity of 2-20, a difference of 1-1,5 V between the frontier molecular orbitals is observed, whereas for clusters with nuclearity of 20-40 this value goes down to 0,20-0,30 V.

Additional factors that take part into the electron counting anomaly and make clusters multivalent, that is being stable to exist with different electron counting but maintaining the same molecular structure, are: a highly packed ligand shell, to avoid the condensation of the cluster upon oxidation; the presence of post-transition heteroatoms, to strengthen the metallic core and avoid its decomposition when in reduced state; the presence of a non-bonding or weakly antibonding orbital into the HOMO-LUMO gap, able to either accept or donate electron density without destabilizing the cluster.

Transition-metal carbonyl clusters can be synthesized following four different pathways: [6]

1. Reductive carbonylation

   The carbonylation pathway involves the reaction between the metal, grinded into a very fine powder, and carbon monoxide. Despite its apparent simplicity, it appears to effectively be appliable only for nickel and iron, giving rise to $Ni(CO)_4$ and $Fe(CO)_5$. In order to obtain metal carbonyl compounds of other metals, reductive carbonylation must be applied. This involves the reaction between an inorganic salt of the chosen metal, carbon monoxide and a reducing agent. The outcome is generally a neutrally-charged metal carbonyl species, such as $Cr(CO)_6$, $Mn_2(CO)_{10}$, $Ru_3(CO)_{12}$, $Co_2(CO)_8$ and $Rh_4(CO)_{12}$.

2. Thermal pathways

   This is a rather straightforward procedure that involves partial decarboxylation though heating of low-nuclearity precursor clusters, followed by condensation of the unsaturated species that results into the formation of new metal-metal bonds.

$$3Rh_4(CO)_{12} \leftrightarrows 2Rh_6(CO)_{16} + 4CO$$

   Sometime, the removal of CO ligands from the precursor leads to an intermolecular rearrangement of the cluster, resulting in no changes in nuclearity.

3. Redox pathways

   The reduction of a cluster often comprises the cleavage of a metal-metal bond or the loss of CO ligands as a result of the addition of electrons to an antibonding orbital. The reduction and consequent loss of a CO ligand could also be induced by the hydroxide ion; the resulting unsaturated species might condensate and assemble into higher nuclearity structures. The oxidation of a cluster exploiting non-coordinating reagents, such as the tropylium cation or the tetrafluoroborate anion, may generate new metal-metal bonds with or without the loss of CO ligands. If coordinating oxidating agents are employed, the complexity of the reaction will increase. Reactions between metal carbonyl clusters and salts or metal complexes can lead to the formation of bimetallic clusters through a "*redox condensation*". [7] This definition was conceived by Paolo Chini, one of the pioneers of the carbonyl cluster chemistry and most esteemed scientist, so as to describe the type of reactions that develops when a cluster is generated from two precursor with different oxidation states.

$$[Fe_3(CO)_{11}]^{2-} + Fe(CO)_5 \leftrightarrows [Fe_4(CO)_{13}]^{2-} + 3CO$$

The redox condensation is perhaps the most straightforward pathway in order to synthesize high-nuclearity metal carbonyl clusters. By employing a salt or a metal complex as the oxidizing agent, it is possible to obtain either homometallic or heterometallic clusters.

4. Other chemically induced pathways

   Metal carbonyl clusters can be modified and, therefore, exploited as a starting point in the synthesis of new species. Besides acids, bases, oxidizing and reducing agents, both anionic and neutral nucleophiles can be employed; these species can either link themselves to the cluster, degrade it, or induce its condensation leading to the formation of higher-nuclearity species. Nucleophilic addition, generally followed by the removal of MLx fragments, is the most recurrent reaction. This way high-nuclearity metal carbonyl clusters can be degraded to smaller species.

2. STATE OF THE ART

This project is focussed on the synthesis and characterization of bimetallic carbonyl clusters of rhodium and gold.

Rhodium carbonyl clusters are compounds that have been studied for many years now; multiple examples of low nuclearity species [8] (maximum 6 metal atoms), medium nuclearity species (between 6 and 12 metal atoms), and high nuclearity species (13 metal atoms or more) can be easily found in chemical literature. Due to its high metal-metal bond energy, [9] rhodium is able to produce high nuclearity homometallic compounds. One of the most notorious structure is $[Rh_{33}(CO)_{47}]^{5-}$, [10] which can be seen in Figure 1, which sets the record for the highest nuclearity among rhodium carbonyl clusters.

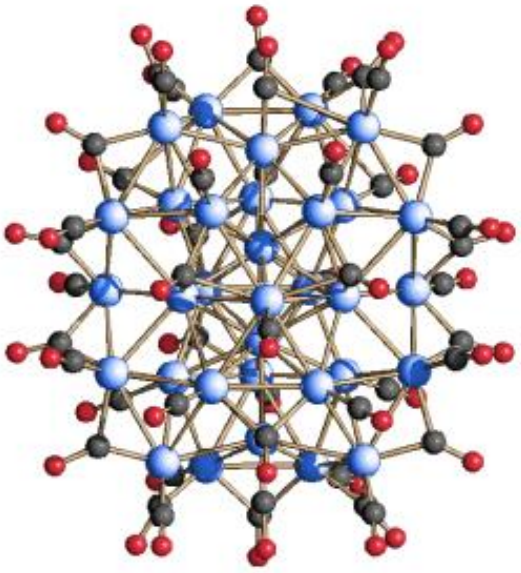

Figure 1: Molecular structure of $[Rh_{33}(CO)_{47}]^{5-}$. Rhodium atoms are represented in blue, carbon atoms are in grey, oxygen atoms are in red.

Rhodium clusters exist also in high-nuclearity heterometallic species including an extensive range of heteroatoms such as C, [11] N, [12] P, [13, 14] S, [15] As, [16] Sn, [17] Sb, [18, 19, 20] Bi [21] and Ge, [20, 22, 23] as well as block-d metals. [24]

As for gold, multiple research projects focussed on heteroatomic M-Au clusters were mostly developed between the Eighties and the Nineties. [25]

The established synthetic pathways and strategies are mainly based on gold complexes with an Au oxidation state of either +1 or +3, although gold behaviour is highly different between the two. The reaction between a homo- or bi-metallic cluster and an Au complex that carries strong ligands (e.g., phosphines) results in a simple addition of the latter to the metal surface, as reported in Figure 2. The reaction pathway includes an interaction between a soft Lewis acid (gold complex) and a soft Lewis base (metallic cluster).

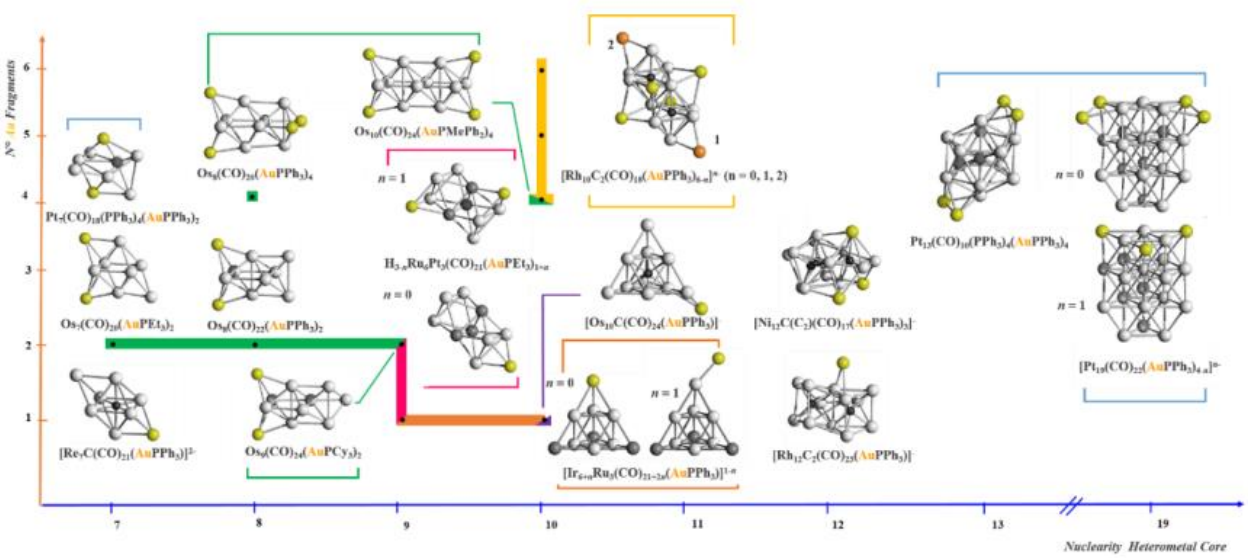

Figure 2: Backbone of the M-Au clusters capped by Au fragments. The gold atoms are represented in yellow.

The most exploited Au^{+} complexes are the ones presenting allyl or aryl phosphines as ligands with either a halogen (such as Cl^{-}) or a non-coordinating ion (such as $[BF_4]^{-}$ or $[PF_6]^{-}$) as counterion. Recently, the possibility to synthesize clusters with gold-carbene complexes as ligands, in the Au-NHC fashion, has been explored. Despite this, multiple cases are known where the $[AuL]^{+}$ fragment coordination to the metal cluster causes a rearrangement of the metal backbone. The cluster stability reaches particularly high values when metals from the second and third transition series are included, since they generate strong M-M bonds, while as for first transition series metals, especially Co and Ni, carbides and nitrides are frequently employed to stabilize the metal core. Moreover, a variation of the structure might take place when bidentate fragments are added to the metal structure. In these cases, it is possible to synthesize dimeric structures where gold acts as a bridge between the two subunits of the cluster (Figure 3).

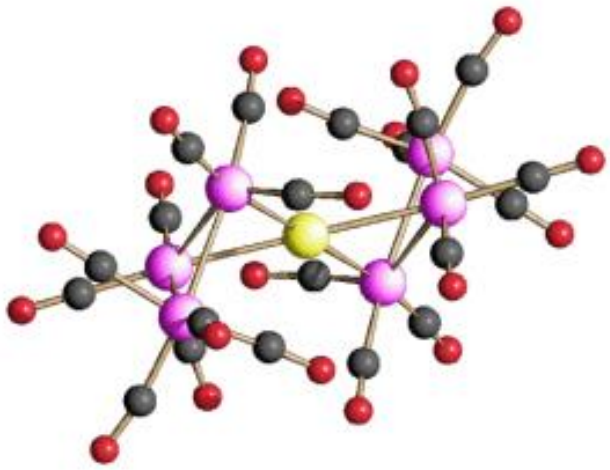

Figure 3: Molecular structure of $[\{HOs_3(CO)_{10}\}_2Au]^{-}$. Osmium atoms are represented in pink, gold atoms are in yellow, carbon atoms are in grey, oxygen atoms are in red.

By exploiting Au(I) complexes with weak ligands, such as halogens or sulphides, or Au(III) complexes, it is possible to synthesize species where gold is incorporated into the metal cluster after being formerly reduced to the oxidation

state 0. This synthesis follows the "*redox condensation*" pathway, as previously described. Moreover, if two or more gold atoms are part of the metal frame, they lean to bond with each other. This phenomenon, known as aurophilicity, [26, 27] leads towards the formation of clusters where gold is encapsulated inside a metal cage derived from the precursor metal cluster (Figure 4).

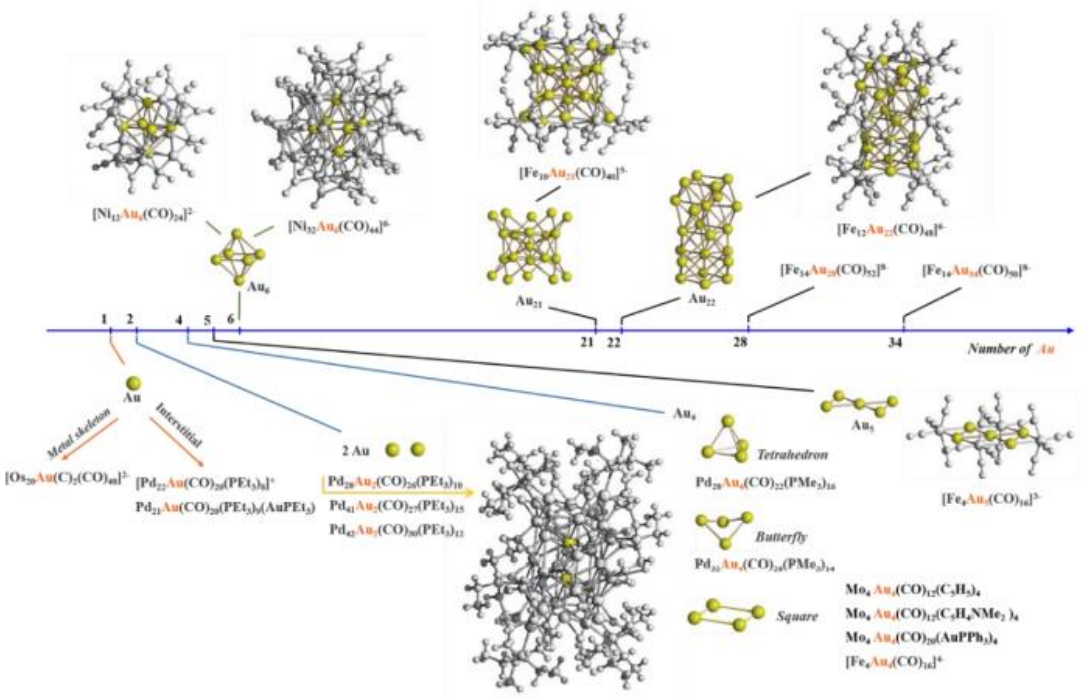

Figure 4: Metal backbone of clusters encapsulating gold inside their metal cage.
The gold atoms are represented in yellow.

Several clusters based on Au-Fe, Au-Pd and Au-Ni compounds are available in chemical literature, but no bimetallic Au-Pt and Au-Rh carbonyl species are known. Only the $[Rh_{16}Au_6(CO)_{36}]^{6-}$ cluster was previously synthesized by the research group in the laboratory. In light of this, the thesis project was focused on the synthesis and characterization of new Au-Rh carbonyl clusters.

The chemistry of Ni-Au carbonyl clusters serves as a guideline for the synthesis of Au-Rh species. In fact, synthetic pathways aimed at synthesizing Ni-Au clusters often start from low nuclearity structures, such as the dianion $[Ni_6(CO)_{12}]^{2-}$, whose Rh equivalent is represented by the $[Rh_7(CO)_{16}]^{3-}$ anion, the starting point for most rhodium cluster syntheses.

Starting from the nickel salt $[PPh_3Me]_2[Ni_6(CO)_{12}]$, dissolved in THF, it is possible to synthesize the $[Ni_{12}Au_6(CO)_{24}]^{2-}$ [28] cluster via a 18h reaction with a Au(I) complex, $AuPPh_3Cl$, in the same solvent, added dropwise, under controlled N_2 atmosphere. This new cluster is formed via an unexpected bond-scission of the PPh_3 ligand from the gold precursor, resulting in a central octahedron of gold atoms which is capped on each of four alternating faces by a triangular $Ni_3(CO)_3(\mu_2\text{-}CO)_3$ ligand in a pseudo-octahedral configuration (Figure 5). The product of interest is extracted in THF and crystallized as $[PPh_3Me]^+$ salt by layering with diisopropyl ether.

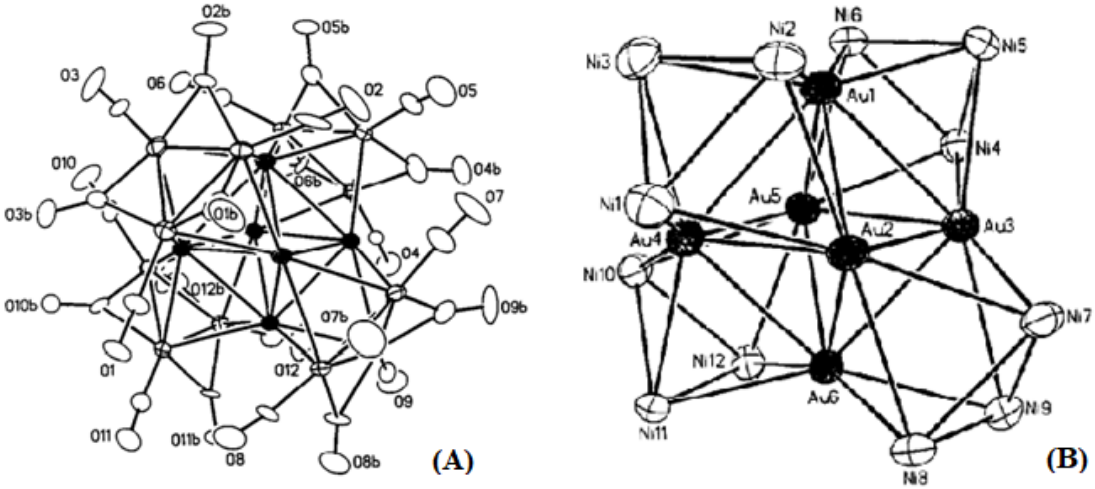

Figure 5: (A) Molecular structure of $[Ni_{12}Au_6(CO)_{24}]^{2-}$ and (B) structure of the metallic backbone of $[Ni_{12}Au_6(CO)_{24}]^{2-}$. Gold atoms are represented in black, nickel atoms are in white.

This cluster represents one of the first example of an organometallic approach to gold nanoparticles.

Moreover, starting from the nickel salt $[NEt_4]_2[Ni_6(CO)_{12}]$, it is possible to synthesize also the $[Ni_{12}Au(CO)_{24}]^{3-}$ [29] and $[Ni_{32}Au_6(CO)_{44}]^{6-}$ [29] clusters via a 1h reaction with a Au(III) species, namely $[NEt_4][AuCl_4]$, in acetone, under controlled N_2 atmosphere. The formation of these clusters happens almost selectively at different Ni_6:Au^{3+} stoichiometric ratios. For the Ni_6:Au^{3+} stoichiometric ratio of 1:0.67, the reaction equation is presumed to be:

$$6[Ni_6(CO)_{12}]^{2-} + 4[AuCl_4]^- \longrightarrow 2[Ni_{12}Au(CO)_{24}]^{3-} + 2Au + 3Ni^{2+} + 9Ni + 16Cl^-$$

The $[Ni_{12}Au(CO)_{24}]^{3-}$ cluster is purified by washing with H_2O, toluene, and THF, then it is extracted in acetone and crystallized as $[NEt_4]^+$ salt via slow diffusion of isopropyl alcohol. This cluster can be structurally described as an asymmetric cell composed by two different $[Ni_6(\mu\text{-}CO)_6(CO)_{16}]^{2-}$ units coordinated to a central Au^+ atom (Figure 6).

The first $[Ni_6(\mu\text{-}CO)_6(CO)_{16}]^{2-}$ unit adopts a distorted octahedral geometry while the second $[Ni_6(\mu\text{-}CO)_6(CO)_{16}]^{2-}$ unit adopts a distorted square pyramid geometry, showing how the $[Ni_6(CO)_{12}]^{2-}$ unit is flexible and able to change its structure when coordinated to a metallic site.

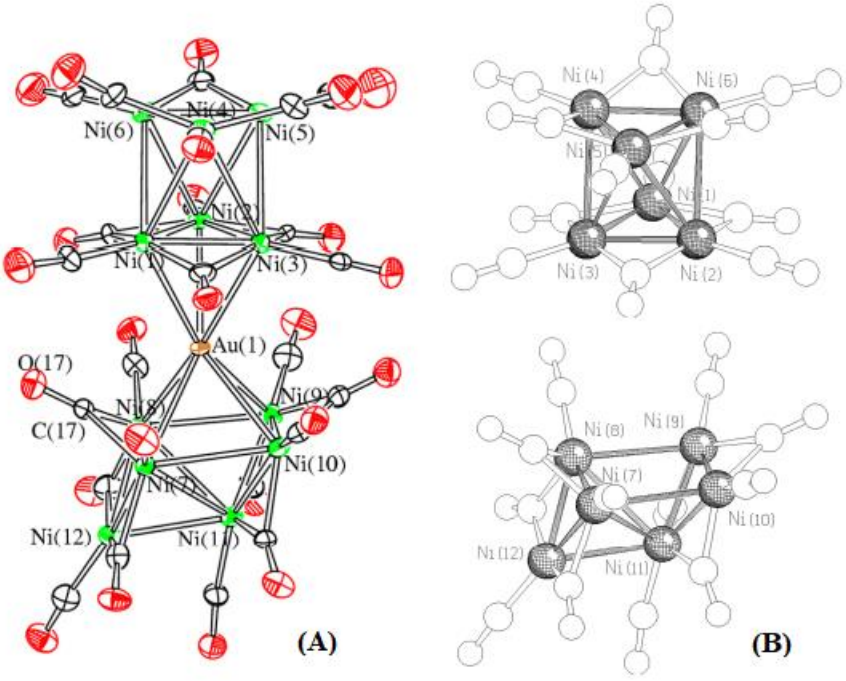

Figure 6: (A) Molecular structure of $[Ni_{12}Au(CO)_{24}]^{3-}$ and (B) structure of the two different $[Ni_6(\mu\text{-}CO)_6(CO)_{16}]^{2-}$ units contained in $[Ni_{12}Au(CO)_{24}]^{3-}$. Nickel atoms are represented in green, gold atoms are in orange, carbon atoms are in black, oxygen atoms are in red.

For the Ni_6:Au^{3+} stoichiometric ratio of 1:0.9, the reaction equation is presumed to be:

$$7[Ni_6(CO)_{12}]^{2-} + 6[AuCl_4]^- \longrightarrow [Ni_{32}Au_6(CO)_{44}]^{6-} + 5Ni^{2+} + 5Ni(CO)_4 + 2CO + 24Cl^-$$

The $[Ni_{32}Au_6(CO)_{44}]^{6-}$ cluster is purified by washing with H_2O, toluene, THF, and acetone, then it is extracted in CH_3CN and crystallized as $[NEt_4]^+$ salt by layering with diisopropyl ether. This cluster can be structurally described as an octahedral Au_6 core surrounded by a Ni_{32} cage (Figure 7).

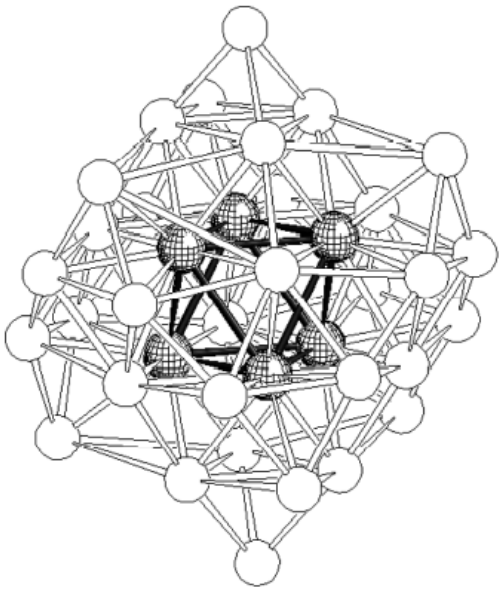

Figure 7: Structure of the metallic backbone of $[Ni_{32}Au_6(CO)_{44}]^{6-}$. Gold atoms are represented in black, nickel atoms are in white.

In agreement with the balanced equations for the latter reactions, $[Ni_{12}Au(CO)_{24}]^{3-}$ can be converted into $[Ni_{32}Au_6(CO)_{44}]^{6-}$ via addition of $[AuCl_4]^-$ or via acidification of the solution with HBF_4.

3. AIM OF THE PROJECT

The aim of this project was to synthesize and characterize new high-nuclearity bimetallic clusters of rhodium and gold.

The $[Rh_7(CO)_{16}]^{3-}$ cluster was chosen as a starting point and it was reacted with both Au(III) and Au(I) species through redox condensations.

All the reactions were run under controlled CO atmosphere. Different stoichiometric ratios between rhodium and gold species were applied so as to verify if different pathways and results could be achieved.

4. RESULTS AND DISCUSSION

The $[Rh_7(CO)_{16}]^{3-}$ cluster has been exploited as an optimal starting point in order to synthesize higher nuclearity rhodium clusters through a redox condensation reaction with different salts. Specifically, in this project the following Au(I) and Au(III) salts were chosen:

- **Au(III)**: $[AuCl_4]^-$ with different counterions, such as tetraethylammonium (TEA^+), tetrabutylammonium (TBA^+) and trimethyl-butylammonium ($TMBA^+$)
- **Au(I)**: $Au(Et_2S)Cl$.

The $[Rh_7(CO)_{16}]^{3-}$ cluster can be easily synthesized starting from another cluster, $Rh_4(CO)_{12}$, by reaction with an excess of KOH under CO atmosphere.

4.1 Synthesis of the reagents

❖ $Rh_4(CO)_{12}$ synthesis

The synthetic pathway for the synthesis of $Rh_4(CO)_{12}$ is a well-known reaction developed almost 50 years ago. The process, which is straightforward and easily reproducible, consists of a treatment of an aqueous solution of $RhCl_3$ with active Cu under CO atmosphere, which is continuously fluxed inside the reaction vessel. $RhCl_3$ can be conveniently obtained commercially.

$$RhCl_3 + 2Cu + 2CO + Cl^- \rightarrow [Rh(CO)_2Cl_2]^- + 2CuCl$$

$$4[Rh(CO)_2Cl_2]^- + 6CO + 2H_2O \rightarrow Rh_4(CO)_{12} + 2CO_2 + 4Cl^- + 4HCl$$

Figure 8: Equipment for $Rh_4(CO)_{12}$ synthesis.

The copper acts as a reducing agent, switching its oxidation state from 0 to +1, while reducing the rhodium's oxidation state from +3 to 0, via a Rh(I) complex. The CO atmosphere is a key factor for the attainment of the reaction, since it favours the formation of the $Rh_4(CO)_{12}$ cluster while preventing the formation of rhodium in metal form. Therefore, it is fundamental to keep the solution under vigorous stirring so as to promote the CO dissolution into the solvent. As the reaction proceeds, the formation and accumulation of HCl will eventually lead to a pH drop. To avoid that, a solution of sodium citrate is added after about 8h from the start, generating a buffer solution which upholds the pH at a value of approximately 4. After around 24h, the reaction is stopped and the $Rh_4(CO)_{12}$ is filtered, extracted in CH_2Cl_2, dried and kept under CO atmosphere.

The compound $Rh_4(CO)_{12}$ is a dark-red solid when crystalline, and orange under powder form. It decomposes under nitrogen at 130-140°C, but the same decomposition also occurs at room temperature on a slower rate. Therefore, $Rh_4(CO)_{12}$ is best stored under a CO atmosphere. [30] The $Rh_4(CO)_{12}$ structure (Picture 9) is described by a tetrahedral array of four Rh atoms stabilized by twelve CO ligands, nine in terminal position and three in edge-bridging position.

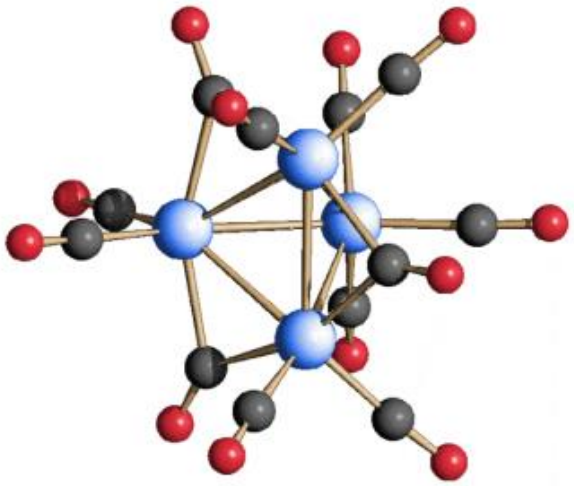

Figure 9: Molecular structure of $Rh_4(CO)_{12}$. Rhodium atoms are represented in blue, carbon atoms are in grey, oxygen atoms are in red.

❖ $[Rh_7(CO)_{16}]^{3-}$ synthesis

The synthesis of $[Rh_7(CO)_{16}]^{3-}$ is a 24-hour process starting from $Rh_4(CO)_{12}$ which is reacted with a large excess of KOH (stoichiometric ratio of 1:30 as reported in the literature) in methanol and under CO atmosphere. It is fundamental to run the reaction under an alkaline environment in order to avoid the formation of the $[Rh_6(CO)_{15}]^{2-}$.

$$7Rh_4(CO)_{12} + 12OH^- \rightarrow 4[Rh_7(CO)_{16}]^{3-} + 14CO + 6CO_2 + 6H2O$$

The main product of the above is $[Rh_7(CO)_{16}]K_3$. A solution of different salts can be added to the reaction media so as to promote the precipitation of the cluster via salt metathesis. Different salt options were exploited throughout this project, all with chloride as anion but with different cations such as: TEA^+, TBA^+, $TMBA^+$ and TPA^+ (tetrapropylammonium). After complete precipitation, the cluster is filtered, extracted in CH_3CN and kept under CO atmosphere.

The compound $[Rh_7(CO)_{16}]^{3-}$ is a dark-green solid in both crystalline and powdered state. Its molecular structure consists of a monocapped octahedron exhibiting a ligand with some distortions with respect to the ideal symmetry; intramolecular factors, such as uneven charge distribution among the metal atoms or intra-ligand steric repulsions, may be largely responsible for the cap asymmetry. [31]

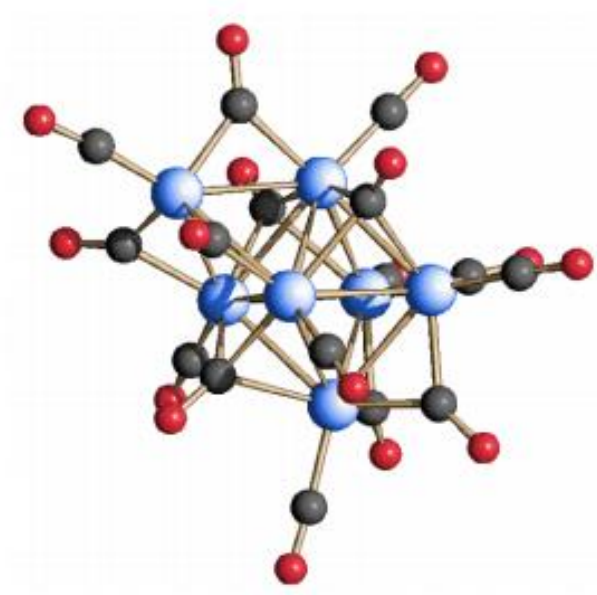

Figure 10: Molecular structure of $[Rh_7(CO)_{16}]^{3-}$. Rhodium atoms are represented in blue, carbon atoms are in grey, oxygen atoms are in red.

4.2 Reactivity of $[Rh_7(CO)_{16}]^{3-}$ with Au in different oxidation states

The behaviour of $[Rh_7(CO)_{16}]^{3-}$ towards oxidation was studied by reacting it with different gold complexes. To start with, its reactivity with a mild oxidating agent, $Au(SEt_2)Cl$, was analysed so as to verify if similar results could be obtained compared to the ones achieved with Au(III).

The reactions were run in different solvents, so as to analyse how their properties could affect the reaction pathways and results. The employment of different cations for the gold salts and $[Rh_7(CO)_{16}]^{3-}$ cluster allowed to obtain the optimal solubility of the reagents into the selected solvents in each case.

The syntheses and results reported below are classified by gold oxidation state and solvent employed in the reactions. Unless otherwise stated, all the procedures were run under controlled CO atmosphere.

4.3 $[Rh_7(CO)_{16}]^{3-}$ + $[AuCl_4]^-$ in DMF

The reactivity of $[Rh_7(CO)_{16}]^{3-}$ and $[AuCl_4]^-$ in DMF as solvent was studied. As a starting point, the reaction was carried out with a Rh_7:Au^{3+} stoichiometric ratio of 1:1. Two separate DMF solutions of $[Rh_7(CO)_{16}][TMBA]_3$ and $[AuCl_4][TMBA]$ were prepared, then the latter solution was added in small amounts (almost 0,2 equivalents) to the former, dropwise, so as to allow a smooth reaction rate. The evolution of the reaction was followed by IR analysis; for the terminal carbonyl region, the formation of an intense peak at 1982s cm^{-1} and two minor peaks at 2008m and 2026m cm^{-1} was observed, while in the bridging carbonyl area, the formation a peak at 1825m cm^{-1} was observed. The reaction was left to react overnight to allow a complete conversion, and the final spectra of the products mixture is reported in Figure 11.

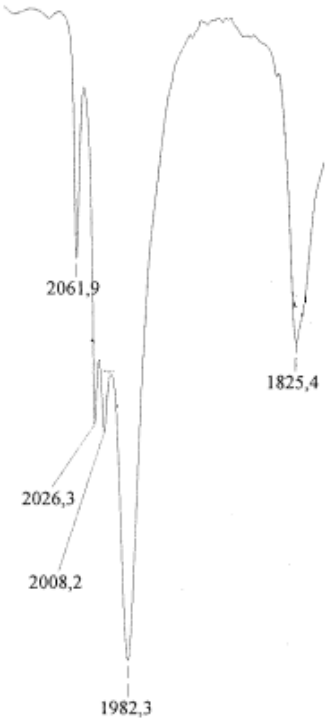

Figure 11: IR spectrum of the products deriving from Rh_7:Au^{3+} 1:1 reaction between $[Rh_7(CO)_{16}]^{3-}$ and $[AuCl_4]^-$ in DMF, under CO atmosphere.

A highly concentrated solution of TMBACl in H_2O was added to the mixture of products in order to favour their precipitation. Then, the precipitate was washed with H_2O so as to remove any excess of salt and dried *in vacuo*.

The solid phase obtained after the drying process, containing a mixture of different products, was purified though work-up: it subsists in a series of consecutive extraction through solvents with increasing polarity. An IR was performed at every single step, so as to identify the products dissolved into every single extraction. The first solvent employed in the process was EtOH, which removes low nuclearity clusters or complexes that might have originated as by-products from the oxidation reaction. As a matter of fact, the IR spectrum displayed two intense peaks in the terminal carbonyl region at 2045vs and 2015vs cm^{-1}, typical of $[Rh_5(CO)_{15}]^-$ cluster. Following up, the extraction in THF solubilized $[Rh_5(CO)_{15}]^-$ still present in the product mixture. The acetone extraction resulted into an unknown IR spectrum with a single intense peak in the terminal carbonyl region at 2010vs cm^{-1}, and three peaks in the bridging carbonyl area at 1857m, 1828m and 1802m cm^{-1}. Taking into consideration the outcome of the spectrum, the solution was layered with hexane so as to favour the crystallization of the clusters included inside. Crystallization results from the gradual diffusion of a nonsolvent into the solution containing the product of interest.

It emerged that, by reacting the species with a Rh_7:Au^{3+} stoichiometric ratio of 1:1, crystals of **$[Rh_{10}Au(CO)_{26}][TMBA]_3$** were obtained in the acetone extraction. The reaction was replicated and its results were proven to be easily reproductible, therefore this was established as main pathway in order to obtain clear crystals of $[Rh_{10}Au(CO)_{26}]^{3-}$. The IR spectrum registered over the crystal solution is reported in Figure 12.

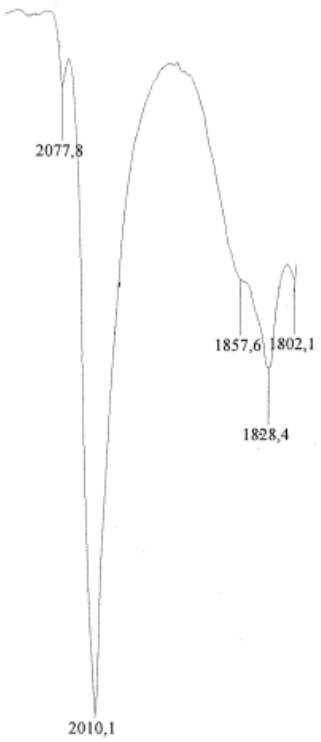

Figure 12: IR spectrum of the solution which resulted in $[Rh_{10}Au(CO)_{26}][TMBA]_3$ crystal formation.

In order to have a more exhaustive understanding of the reaction's behaviour, a new reaction was carried out with a Rh_7:Au^{3+} stoichiometric ratio of 1:2 with TEA^+ as counterion for both the gold and rhodium species.

Running the same procedure as before, the evolution of the reaction was followed by IR analysis; in the terminal carbonyl region, the formation of two intense peaks at 2062s cm^{-1} and 1983vs cm^{-1} was observed, while in the bridging carbonyl area, the formation of a double peak at 1824m cm^{-1} and 1817m cm^{-1} was observed. The reaction was left to develop overnight, and the final spectrum of the product mixture is reported in Figure 13.

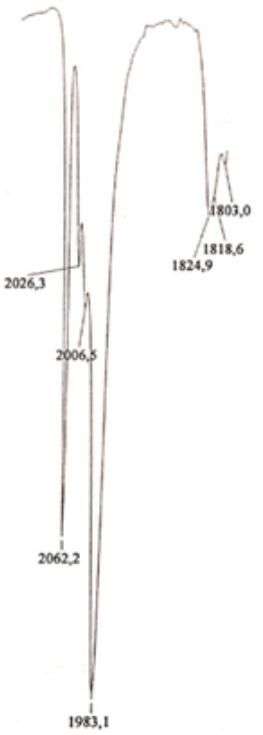

Figure 13: IR spectrum of the products deriving from the Rh_7:Au^{3+} 1:2 reaction between $[Rh_7(CO)_{16}]^{3-}$ and $[AuCl_4]^-$ in DMF, under CO atmosphere.

A highly concentrated solution of TEACl in H_2O was added to the mixture of products in order to favour their precipitation.

Then, the reaction work-up started: EtOH extraction displayed an IR spectrum with two intense peaks in the terminal carbonyl region at 2072vs and 1999s cm^{-1}, typical of the $[Rh(CO)_2Cl_2]^-$ complex, and peaks typical of $[Rh_5(CO)_{15}]^-$ cluster. The THF extraction solubilized the remaining $[Rh_5(CO)_{15}]^-$ cluster. The acetone extraction resulted into an unknown IR spectrum with a very intense peak in the terminal carbonyl region at 2019vs cm^{-1}, with two shoulder-type peaks at 2047sh and 1996sh cm^{-1}, and a peak in the bridging carbonyl area at 1823m cm^{-1}, with two shoulder-type peaks at 1837sh and 1813sh cm^{-1}. The solution was layered in hexane.

The layering of the unknown solution did not result in any crystal formation, but a solid precipitation occurred. Despite various crystallization attempts with different solvents, no crystals suitable for X-ray diffraction were obtained. The IR spectrum of the final recovery acetonitrile solution is reported in Figure 14.

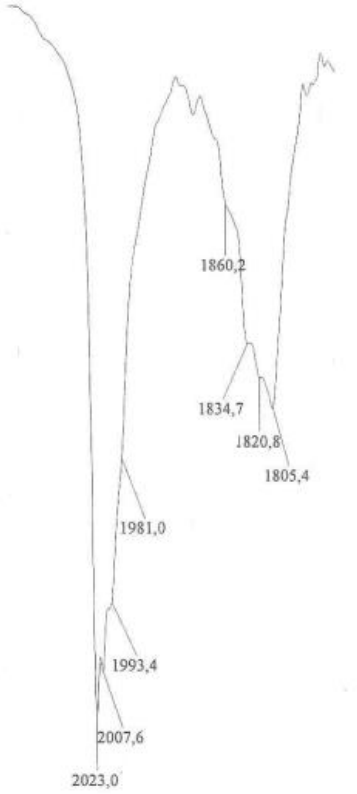

Figure 14: IR spectrum of the former acetone extraction, registered in CH_3CN, at final recovery step.

The latter reaction was performed once again, so as to validate the reproducibility of the results and hopefully achieve crystal formation. The same procedure and conditions as before were applied, but a cation exchange step with TMACl was performed before the work-up to analyse how different counterions might affect the crystallisation process. The final IR displayed the same peaks obtained in the previous reaction. The layering resulted in crystals formation, the analysis through

FT-IR, ESI-MS, and single crystal X-ray diffractometry revealed their composition to be **$[Rh_{16}Au_6(CO)_{36}][TMA]_4$**. The IR spectrum in solution over the crystal solution is reported in Figure 15.

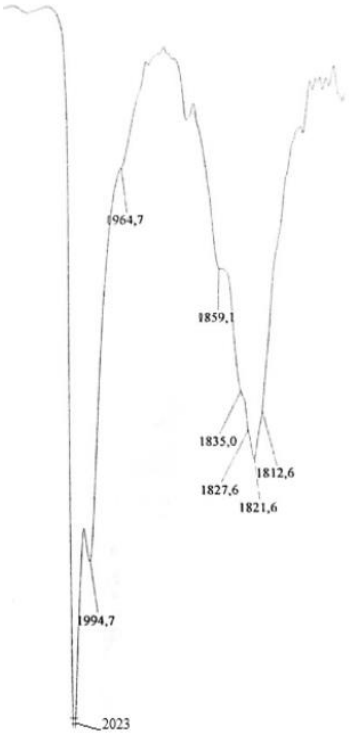

Figure 15: IR spectrum of the solution which resulted in $[Rh_{16}Au_6(CO)_{36}][TMA]_4$ crystal formation.

The same IR spectrum of $[Rh_{16}Au_6(CO)_{36}]^{4-}$ was obtained when the reaction was performed starting from $[Rh_7(CO)_{16}][TMBA]_3$ and $[AuCl_4][TMBA]$ as reagents in the same reaction conditions as before, thus verifying the reproducibility of the synthetic pathway to obtain $[Rh_{16}Au_6(CO)_{36}]^{4-}$.

4.4 $[Rh_7(CO)_{16}]^{3-}$ + $[AuCl_4]^-$ in THF

The reactivity of $[Rh_7(CO)_{16}]^{3-}$ and $[AuCl_4]^-$ in THF as solvent was studied. As a starting point, the reaction was carried out with a Rh_7:Au^{3+} stoichiometric ratio of 1:1. Two separate THF solutions of $[Rh_7(CO)_{16}][TBA]_3$ and $[AuCl_4][TEA]$ were prepared, then latter was added, dropwise, to the former. The evolution of the reaction was followed by IR analysis; the IR spectrum at the end of the reaction displayed an intense peak in the terminal carbonyl region at 1982s cm^{-1}, with two shoulder-type peaks at 2026sh and 2008sh cm^{-1}, and a single peak in the bridging carbonyl area at 1827m cm^{-1}, along with a two shoulder-type peaks at 1807sh and 1771sh cm^{-1}. The spectrum highly resembled the one obtained in the 1:1 reaction in DMF; as a matter of fact, the same peaks are displayed in the terminal carbonyl region, while shoulder-type peaks, that were not displayed in the latter reaction, are present in the bridging carbonyl region. Therefore, the reaction was expected to have come to similar results, along with a higher concentration of by-products. The solution was left to react overnight, and a solid precipitation occurred. The liquid and solid phases were separated, both dried *in vacuo* and the work-up was started.

The liquid phase was dried *in vacuo* and extracted in EtOH, resulting in an IR spectrum with peaks typical of the $[Rh(CO)_2Cl_2]^-$ complex and $[Rh_5(CO)_{15}]^-$ cluster. The CH_2Cl_2 extraction displayed a clean $[Rh_{10}Au(CO)_{26}]^{3-}$ IR spectrum. Therefore, the CH_2Cl_2 solution was dried *in vacuo* and kept to test the cluster reactivity.

Since the solid phase precipitated in THF, after filtration it was washed with H_2O and then it underwent work-up. The first solvent employed for the procedure was acetone, which resulted in an IR spectrum with an intense peak in the terminal carbonyl region at 2005s cm^{-1}, with a shoulder-type peak at 1986sh cm^{-1}, and two peaks in the bridging carbonyl area at 1825m and 1803m cm^{-1}. The IR spectrum is reported in Figure 16.

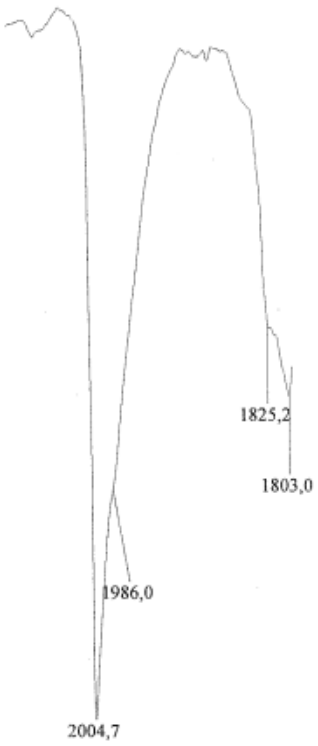

Figure 16: IR spectrum of the acetone extraction.

The extraction was layered in hexane, resulting in no crystal formation, but a solid precipitation occurred. The solid was recovered, dried *in vacuo*, dissolved in CH_3CN, and layered in hexane and diisopropyl ether. A crystal formation was observed, the analysis through FT-IR, ESI-MS, and single crystal X-ray diffractometry confirmed their composition to be **$[Rh_{16}Au_6(CO)_{36}][TEA]_6$** cluster, while the presence of **$[Rh_{10}Au(CO)_{26}]^{3-}$** cluster was detected only in solution. Although both TBA^+ and TEA^+ were present in the reaction solution, with a TBA^+:TEA^+ stoichiometric ratio of 3:1, the analysed crystal contained only TEA^+ as counterion. As a matter of fact, TEA^+ was found to lower the $[Rh_{16}Au_6(CO)_{36}]^{6-}$ solubility, thus allowing it to precipitate out of the solution. The IR spectrum over the solution containing the crystals is reported in Figure 17.

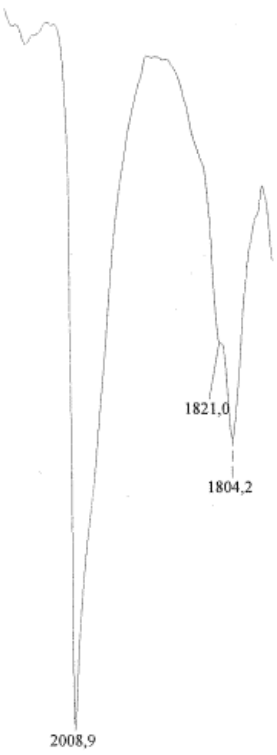

Figure 17: IR spectrum of the solution which resulted in $[Rh_{16}Au_6(CO)_{36}]^{6-}$ crystal formation.

In order to have a more comprehensive understanding of the reaction's behaviour, a new reaction was carried out with a Rh_7:Au^{3+} stoichiometric ratio of 1:0.5.

Running the same procedure as before, the IR spectrum at the end of the reaction displayed the same peaks as the 1:1 reaction. The solution was left to react overnight, and a solid precipitation occurred. The liquid and solid phases were separated, then the liquid phase was precipitated with the addition of a highly concentrated solution of TEACl in H_2O, dried *in vacuo*, washed with H_2O to remove any excess of salt and dried again. The work-up started, an IR analysis was performed on each step.

The solid phase was extracted in acetone, resulting in an IR spectrum similar to the one of the $[Rh_{10}Au(CO)_{26}]^{3-}$ cluster. The solution was layered in hexane, but no

crystal formation was observed, preventing from having an unambiguous confirmation of its identity.

The liquid phase was washed with EtOH, the IR spectrum displayed the presence of the $[Rh_5(CO)_{15}]^-$ cluster. The following CH_2Cl_2 and THF extractions resulted in extremely similar IR spectra, displaying an intense peak in the terminal carbonyl area at 2010vs cm^{-1}, along with a minor peak at 2040m cm^{-1}, and two peaks in the bridging carbonyl region at 1826m and 1803m cm^{-1}. Therefore, these two extractions were merged, dried *in vacuo* and dissolved in MeOH. The spectra are reported in Figure 18.

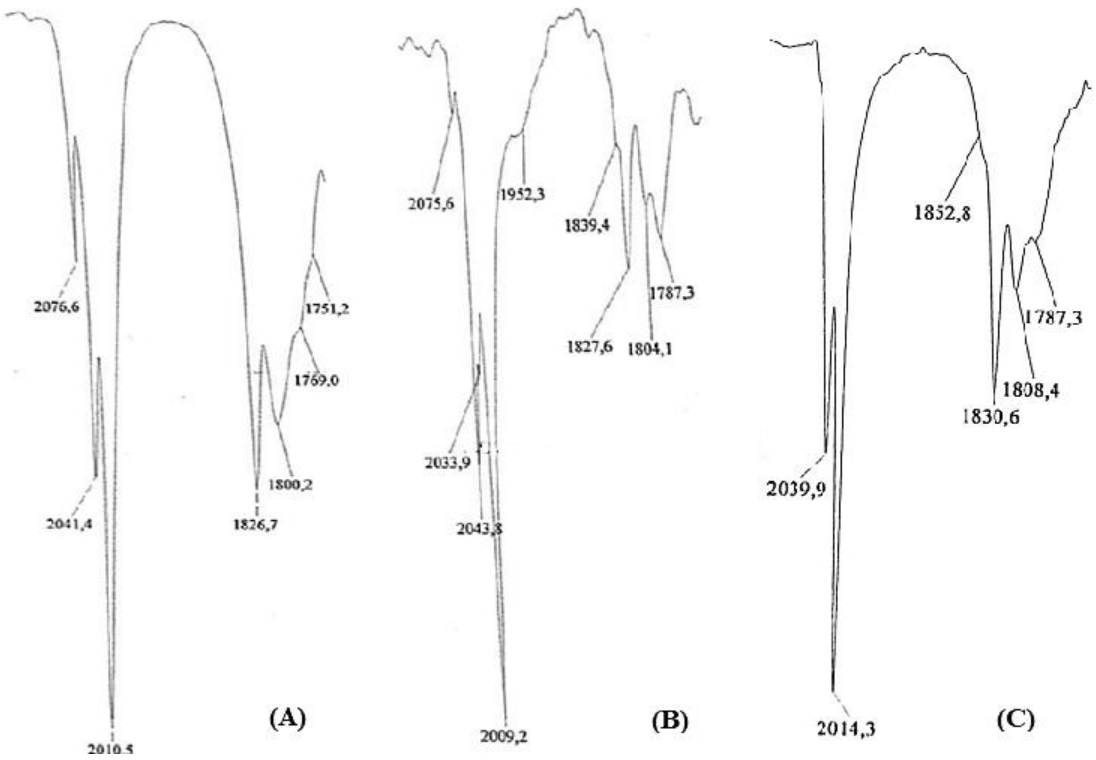

Figure 18: IR spectra of (A) the CH_2Cl_2 extraction, (B) the THF extraction and (C) the MeOH solution.

The FT-IR analysis over the solution detected the presence of the **$[Rh_{10}Au(CO)_{26}]^{3-}$** cluster as main product of the reaction, although any crystallization attempt failed.

4.5 Reactivity of $[Rh_{10}Au(CO)_{26}]^{3-}$

The results listed above, in both DMF and THF, led to the hypothesis that the formation of $[Rh_{16}Au_6(CO)_{36}]^{4-}$ could be a consecutive reaction starting from $[Rh_{10}Au(CO)_{26}]^{3-}$. As a matter of fact, at lower Rh_7:Au^{3+} stoichiometric ratios the formation of $[Rh_{10}Au(CO)_{26}]^{3-}$ appeared to be favoured, while at higher Rh_7:Au^{3+} stoichiometric ratios the formation of $[Rh_{16}Au_6(CO)_{36}]^{4-}$ appeared to be favoured. In order to verify the accuracy of this hypothesis, or otherwise prove that the formation of these two species is not connected, different reactivity test were run over $[Rh_{10}Au(CO)_{26}]^{3-}$.

The $[Rh_{10}Au(CO)_{26}]^{3-}$ solution obtained from the 1:1 reaction between $[Rh_7(CO)_{16}]^{3-}$ and $[AuCl_4]^-$ in THF was employed to test this hypothesis. The solution was divided in two units, each one employed in a different reactivity test.

The first portion was dried *in vacuo* and dissolved into DMF, then 1 eq. of $[AuCl_4][TMBA]$ in DMF was added dropwise, so as to reach an overall Rh_7:Au^{3+} stoichiometric ratio of 1:2. The IR spectrum (Figure 19) displayed an intense peak in the terminal carbonyl region at 1983vs cm^{-1} with a minor peak at 2008s cm^{-1}, and two peaks in the bridging carbonyl area at 1826m cm^{-1} and 1802m cm^{-1}.

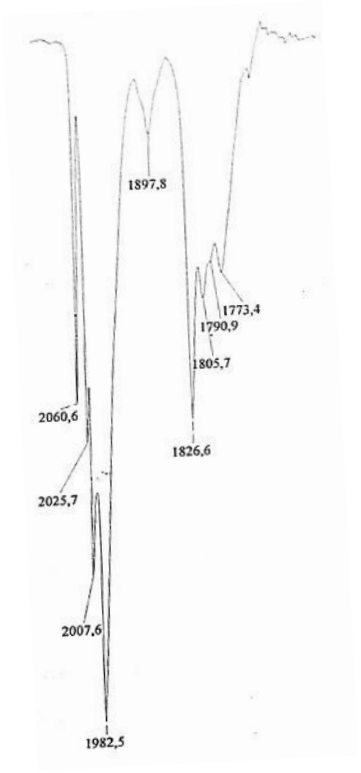

Figure 19: IR spectrum of the solution at the end of the reaction.

The work-up started; the THF extraction was the only remarkable one, displaying an interesting but highly diluted IR spectrum. Therefore, the solution was dried *in vacuo*, and dissolved into a small amount of acetone, then layered in hexane in order to favour the crystallization process. No crystals were obtained, even when the solution was recovered in CH_3CN. However, through the analysis of the obtained IR spectra, it was possible to identify the presence of the **$[Rh_{16}Au_6(CO)_{36}]^{4-}$** cluster in solution, thus attesting how the formation of this cluster actually follows a consecutive pathway starting from $[Rh_{10}Au(CO)_{26}]^{3-}$.

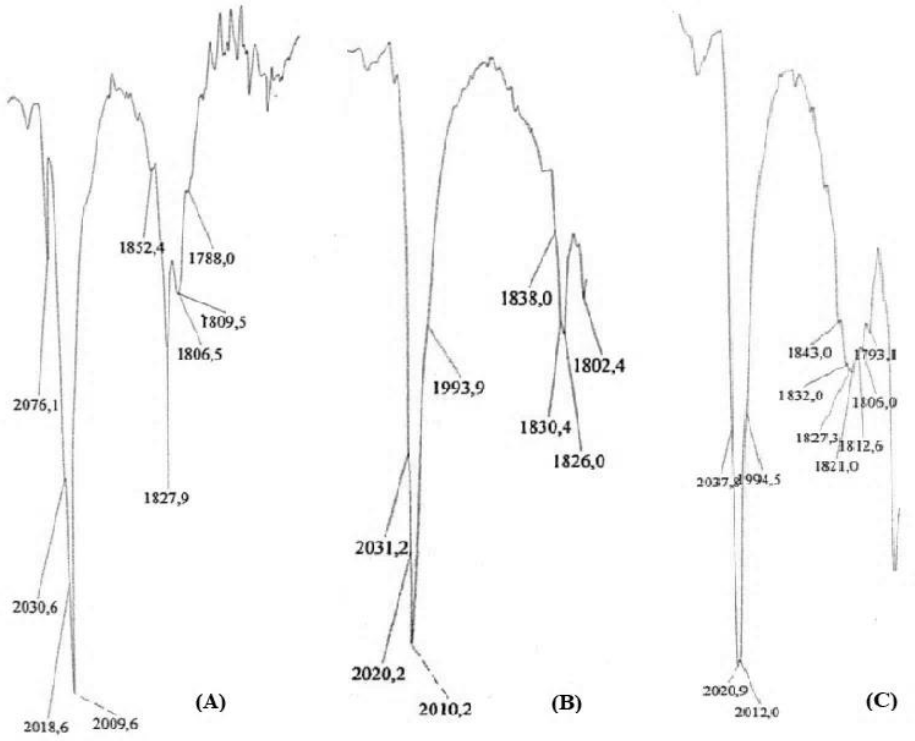

Figure 20: IR spectrum of (A) the THF extraction, (B) the recovery of the solution in acetone and (C) the recovery of the solution in CH_3CN.

The nuclearity of rhodium clusters is known to increase when in acidic environments, due to oxidation reactions, therefore it was analysed if $[Rh_{10}Au(CO)_{26}]^{3-}$ could convert to $[Rh_{16}Au_6(CO)_{36}]^{4-}$ when acidified. Therefore, the second unit of the starting solution was dried *in vacuo* and dissolved into CH_2Cl_2, then the solution was acidified with the addition of HBF_4. The IR spectrum displayed an intense peak in the terminal carbonyl region at 2031s cm^{-1}, along with a shoulder-type peak at 1994sh cm^{-1}, and three peaks in the bridging carbonyl area at 1863m, 1835m and 1815m cm^{-1} (Figure 21).

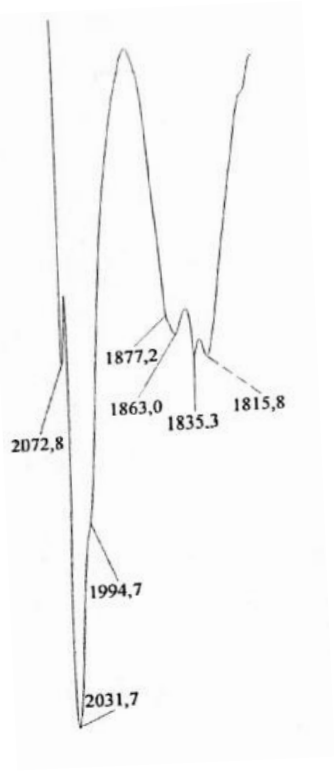

Figure 21: IR spectrum of the solution.

The solution was layered with 2-propanol, but no crystals were obtained. However, through the analysis of the FT-IR spectra and ESI-MS results, it was possible to identify the presence of the **$[Rh_{16}Au_6(CO)_{36}]^{4-}$** cluster in solution. Therefore, the possibility to increase the $[Rh_{10}Au(CO)_{26}]^{3-}$ nuclearity to $[Rh_{16}Au_6(CO)_{36}]^{4-}$ via acidification was confirmed.

4.6 $[Rh_7(CO)_{16}]^{3-}$ + $[AuCl_4]^-$ in acetone

The reactivity of $[Rh_7(CO)_{16}]^{3-}$ and $[AuCl_4]^-$ in acetone as solvent was studied to explore how the reaction pathway might change, since acetone is a non-coordinating solvent as THF. A Rh_7:Au^{3+} stoichiometric ratio of 1:1 was selected.

Two separate acetone solutions of $[Rh_7(CO)_{16}][TPA]_3$ and $[AuCl_4][TEA]$ were prepared. The latter was added in small amounts (almost 0,2 equivalents) to the former, dropwise, so as to allow a smooth reaction rate.

The evolution of the reaction was followed by IR analysis; for the terminal carbonyl region, the formation of an intense peak at 1984s cm^{-1} along with multiple shoulder-type peaks at 2008sh and 2026sh cm^{-1} was observed, while for the bridging carbonyl area, the formation of a single peak at 1826m cm^{-1} was observed. The same IR spectrum was obtained at the end of the previous reactions in both DMF and THF. The solution was left overnight to allow any reaction that might still have been happening to come to an end, and the final spectrum of the products mixture is reported in Figure 22.

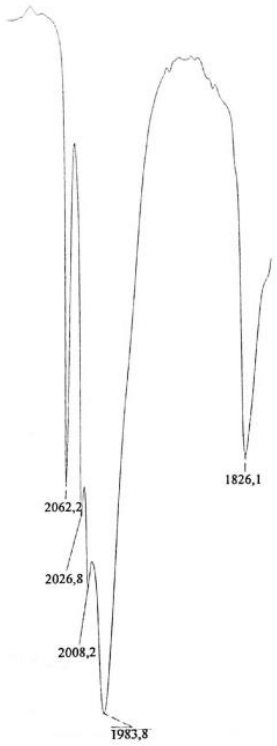

Figure 22: IR spectrum of the products deriving from the reaction between $[Rh_7(CO)_{16}]^{3-}$ and Au(III) in acetone, under CO atmosphere.

The product mixture was dried *in vacuo*, washed with H_2O, dried *in vacuo* and the work-up started; an IR analysis was performed on each step. The first solvent employed was EtOH, the IR spectrum reported peaks typical of the $[Rh(CO)_2Cl_2]^-$ complex. Next, the CH_2Cl_2 extraction resulted in an extremely diluted spectrum, therefore it was considered as non-remarkable. The THF extraction resulted in an IR spectrum typical of the $[Rh_5(CO)_{15}]^-$ cluster. The acetone extraction resulted in a spectrum particularly similar to the one of the $[Rh_{10}Au(CO)_{26}]^{3-}$ cluster, displaying very intense peak in the terminal carbonyl region at 2009vs cm^{-1}, with two shoulder-type peaks at 2020sh and 1997sh cm^{-1}, and a peak in the bridging carbonyl area at 1826s cm^{-1}, with a shoulder-type peak at 1804sh cm^{-1}. The spectrum is reported in Figure 23.

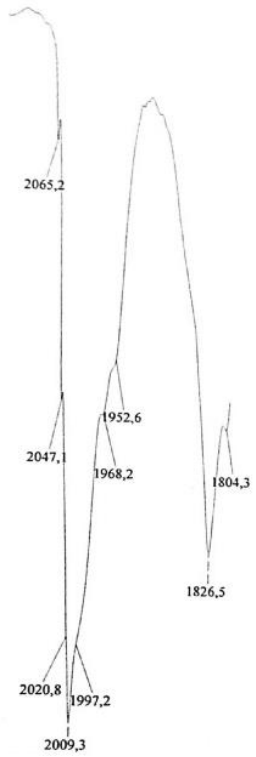

Figure 23: IR spectrum of the acetone extraction.

The wideness of the main peaks and the presence of minor shoulder-type peaks confirmed the presence of multiple species in the solution. The acetone extraction was layered with hexane so as to favour the crystallization of one or more clusters.

The layering of the acetone extraction did not result in the expected outcome: even if the IR spectrum was highly compatible with the one of $[Rh_{10}Au(CO)_{26}]^{3-}$, the obtained crystals, once analysed through X-ray diffractometry, resulted to be composed by $\mathbf{[Rh_{12}(CO)_{30}]^{2-}}$. This already known compound, [32] although being a by-product, preferentially crystallized in the selected layering conditions.

The crystals were separated, and the solution was collected, dried *in vacuo*, and recovered two times: on the first attempt, the solution was re-dissolved in acetone and layered in hexane, but no crystals were obtained; on the second attempt, the solution was dissolved in CH_3CN and layered in hexane and diisopropyl ether.

This time the formation of crystal was observed, and the X-ray analysis allowed to identify the new **$[Rh_{19}Au_5(CO)_{40}][TEA]_2[TPA]_2$** cluster, which was also characterized by IR spectroscopy. Its IR spectrum registered in acetonitrile solution is reported in Figure 24.

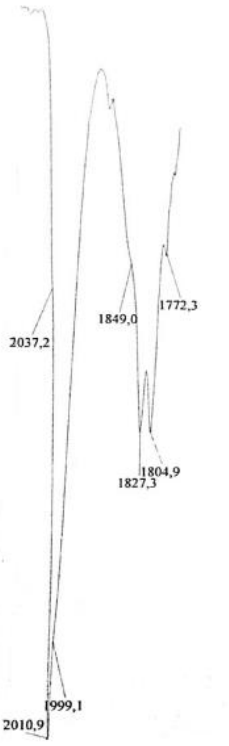

Figure 24: IR spectrum of the solution which resulted in $Rh_{19}Au_5(CO)_{40}][TEA]_2[TPA]_2$ crystal formation.

4.7 $[Rh_7(CO)_{16}]^{3-}$ + $Au(Et_2S)Cl$ in CH_3CN

In order to verify if similar results could be obtained by applying milder oxidating agents, reactions with Au(I) species were run at higher stoichiometric ratios than the previous one, assuming the reactions would follow similar pathways then the already known ones if higher amounts of Au were added.

Two CH_3CN solutions of $[Rh_7(CO)_{16}][TEA]_3$ and $Au(Et_2S)Cl$ were prepared, based on a Rh_7:Au^+ stoichiometric ratio of 1:2.25. Then, the latter was added, dropwise, to the former. The evolution of the reaction was followed by IR analysis; for the terminal carbonyl region, the formation of an intense peak at 1989vs cm^{-1} with shoulder-type peaks at 2010sh and 2032sh cm^{-1} was observed, while for the bridging carbonyl area, the formation of a peak at 1824m cm^{-1} with shoulder-type peaks at 1803sh and 1765sh cm^{-1} was observed. Compared to the IR spectra obtained at the end of the reactions with Au(III) species, the latter displayed similar peaks in the terminal carbonyl region but shifted towards higher wavelengths, while the bridging carbonyl area displayed the usual peak at 1824 cm^{-1}. The reaction was left overnight. The final spectrum of the products mixture is reported in Figure 25.

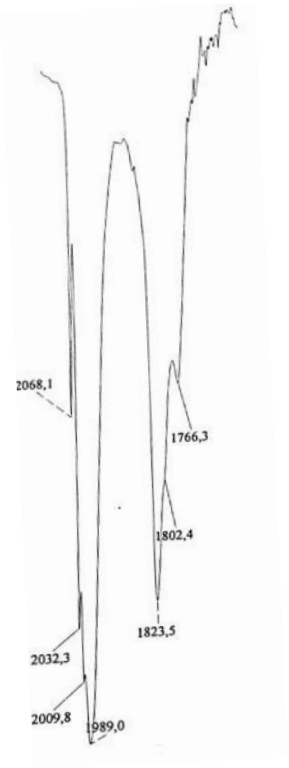

Figure 25: IR spectrum of the products of the reaction between $[Rh_7(CO)_{16}]^{3-}$ and $Au(Et_2S)Cl$ in CH_3CN, under CO atmosphere.

The solution was dried *in vacuo*, washed with H_2O, dried *in vacuo* and the work-up started; an IR analysis was performed on each step.

The EtOH extraction resulted in an IR spectrum displaying peaks typical of the $[Rh(CO)_2Cl_2]^-$ complex and $[Rh_5(CO)_{15}]^-$ cluster. The THF extraction resulted in an IR spectrum typical of the $[Rh_5(CO)_{15}]^-$ cluster. The IR the spectrum over the acetone extraction, reported in Figure 26, revealed the presence of $[Rh_{10}Au(CO)_{26}]^{3-}$ in the solution, along with other by-products. Therefore, it was layered in hexane expecting to get crystals.

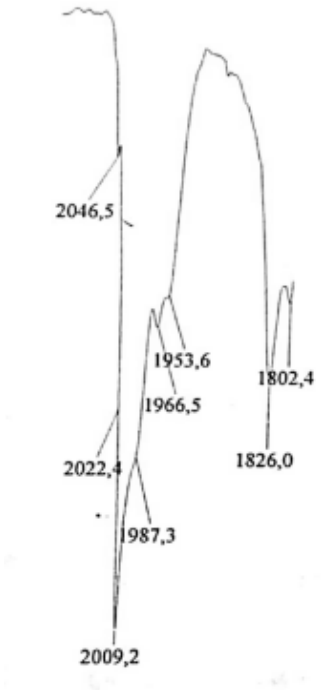

Figure 26: IR spectrum of the acetone extraction.

Although promising, the layering did not result in any crystal formation, but a solid precipitation was observed. The solid was recovered, dried *in vacuo*, dissolved in acetone, and layered in hexane, resulting again in no crystal formation. It was recovered once more, dried *in vacuo,* dissolved in CH_3CN but only a partial dissolution was detected; therefore, liquid and solid were separated, the solution was layered in hexane and diisopropyl ether, while the solid was dissolved in DMF and layered in diisopropyl ether. Only the solution resulted in formation of crystals, which were analysed through IR and X-ray revealing their composition as crystals of a new cluster, **$[Rh_{20}Au_7(CO)_{45}][TEA]_5$.** The IR spectrum over the crystal solution, which appears as the union of the spectra of $[Rh_{10}Au(CO)_{26}]^{3-}$ and $[Rh_{16}Au_6(CO)_{36}]^{4-}$, is reported in Figure 27. The $[Rh_{20}Au_7(CO)_{45}]^{5-}$ cluster is most likely to be a by-product that selectively crystallized in the selected reaction conditions.

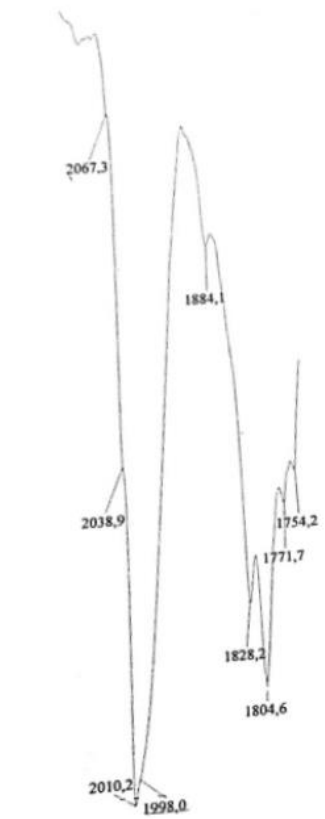

Figure 27: IR spectrum of the CH_3CN solution which resulted in $[Rh_{20}Au_7(CO)_{45}][TEA]_5$ crystal formation.

Furthermore, the reaction was studied at lower Rh_7:Au^+ stoichiometric ratios.

Starting from a 1:2.5 ratios and following alongside the same procedure as before, similar spectra were obtained both at the end of the reaction and in the steps of the work-up procedure. The extraction in acetone was layered in hexane and recovered multiple times, although it did not result in any crystal formation. The IR spectrum showed what seemed to be a mixture of $[Rh_{10}Au(CO)_{26}]^{3-}$, $[Rh_{16}Au_6(CO)_{36}]^{6-}$, $[Rh_{16}Au_6(CO)_{36}]^{4-}$ and $[Rh_{20}Au_7(CO)_{45}]^{5-}$, although it was not possible to get any of these to crystallize.

Supposing that the reaction could selectively move towards one of the single species identified in the previous one, the Rh_7:Au^+ stoichiometric ratio was lowered down to 1:6. In this case the THF extraction resulted in a mixed IR between $[Rh(CO)_2Cl_2]^-$, $[Rh_5(CO)_{15}]^-$, $[Rh_7(CO)_{16}]^{3-}$ and $[Rh_{10}Au(CO)_{26}]^{3-}$ (Figure 28); layering in hexane did not result in any crystal formation, but after recovering the solution in acetone, black crystals of **$[Rh_{10}Au(CO)_{26}][TMBA]_3$** were detected. The acetone extraction gave the same result. (Figure 28).

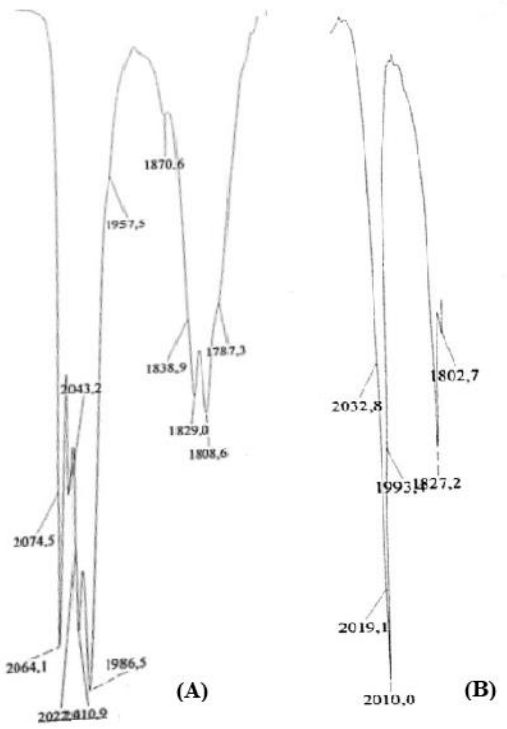

Figure 28: IR spectra of (A) the THF extraction and (B) the crystal solution of $[Rh_{10}Au(CO)_{26}][TMBA]_3$.

4.8 $[Rh_7(CO)_{16}]^{3-}$ + $Au(Et_2S)Cl$ in DMF

The reactivity of $[Rh_7(CO)_{16}]^{3-}$ and $Au(Et_2S)Cl$ in DMF was studied. Solutions of $[Rh_7(CO)_{16}][TMBA]_3$ and $Au(Et_2S)Cl$ in DMF were prepared, based on a Rh_7:Au^+ stoichiometric ratio of 1:3. The gold solution was added entirely to the rhodium solution as, after being dissolved in DMF, its colour started to turn from yellow to reddish; presumably, $Au(Et_2S)Cl$ is unstable in DMF. The reaction was left overnight and an analysed through IR the following morning. The spectrum (Figure 29) displayed an intense peak in the terminal carbonyl region at 1983vs cm-^{1}, along with multiple small shoulder-type peaks at 2000sh, 2009sh, 2025sh and 2038sh cm^{-1}, and a single peak in the bridging carbonyl area at 1826s cm^{-1}. Although the main peaks were similar to the ones obtained at the end of the previously analysed reactions, the presence of such a high number of shoulder-type peaks suggested the presence of a considerable number of by-products.

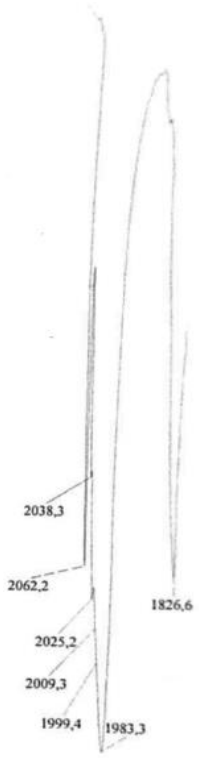

Figure 29: IR spectrum of the products of the reaction between $[Rh_7(CO)_{16}]^{3-}$ and $Au(Et_2S)Cl$ in DMF, under CO atmosphere.

A highly concentrated solution of TMBACl in H_2O was added to favour the precipitation of the products of the reaction. Then, the precipitate was filtered, washed with H_2O, dried *in vacuo* and the work-up started; an IR analysis was performed on each step.

The EtOH extraction resulted in an IR spectrum displaying peaks typical of the $[Rh_5(CO)_{15}]^-$ cluster, as well as the THF. The IR the spectrum over the acetone extraction (Figure 30) displayed peaks typical of the $[Rh_{16}Au_6(CO)_{36}]^{4-}$cluster, therefore it was layered in hexane to promote its crystallization.

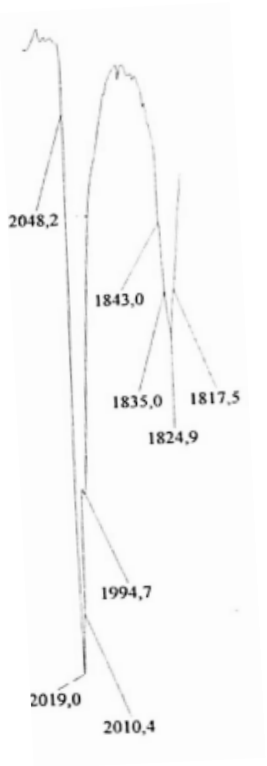

Figure 30: IR spectrum of the acetone extraction.

Crystals were obtained, but their analysis through FT-IR and single crystal X-ray diffraction revealed their composition to be **$[Rh_{10}Au(CO)_{26}][TMBA]_3$**. As a matter of fact, crystals of the same cluster were obtained also in the 1:1 DMF reaction with $[AuCl_4][TMBA]$, thus highlighting the affinity of this product to crystallize in acetone as solvent and with $TMBA^+$ as counterion.

4.9 $[Rh_{10}Au(CO)_{26}]^{3-}$: molecular structure and spectroscopic characterization

The IR spectrum of the crystals dissolved in CH_3CN is reported in Figure 31.

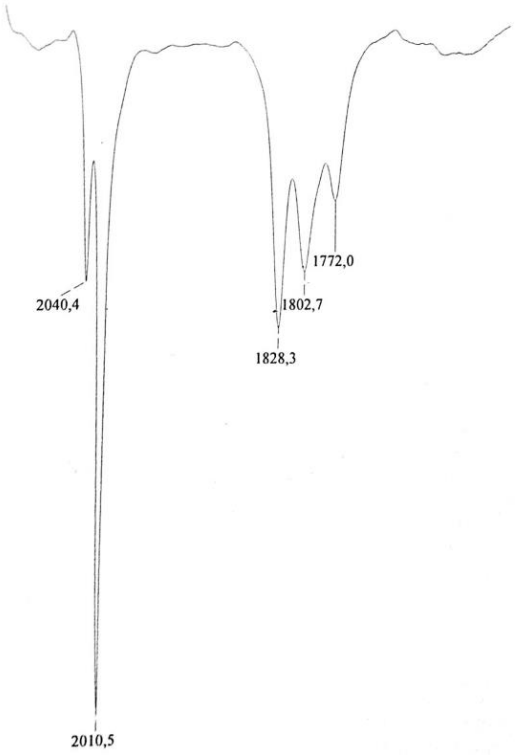

Figure 31: IR spectrum of $[Rh_{10}Au(CO)_{26}]^{3-}$ crystals dissolved in CH_3CN under CO atmosphere.

The spectrum displays a high peak in the terminal carbonyl region at 2010vs cm^{-1}, along with a minor peak at 2040m cm^{-1}, and three peaks in the bridging carbonyl area at 1828m, 1802m and 1772m cm^{-1}.

The molecular structure of $[Rh_{10}Au(CO)_{26}]^{3-}$ (Figure 32) is composed by two Rh_5Au octahedrons sharing the gold atom. A shell of twenty-six carbonyl ligands stabilizes the structure, ten of those in terminal position and sixteen of those in double-bridging position.

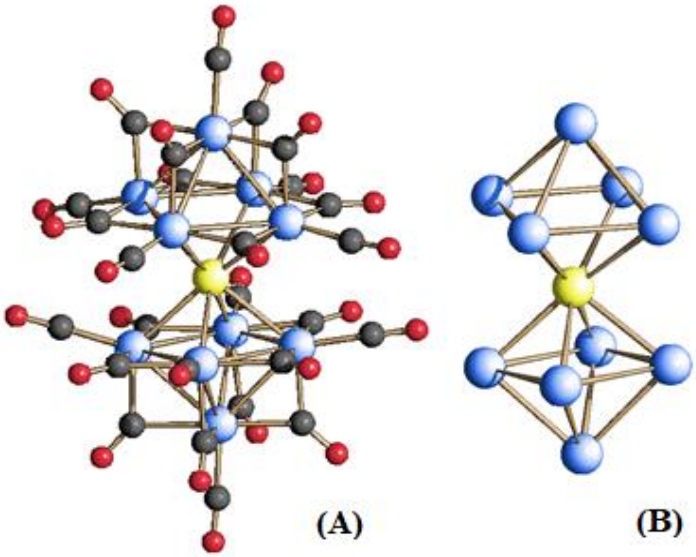

Figure 32: (A) Molecular structure of $[Rh_{10}Au(CO)_{26}]^{3-}$ and (B) structure of the metallic backbone of $[Rh_{10}Au(CO)_{26}]^{3-}$. Rhodium atoms are represented in blue, carbon atoms are in grey, oxygen atoms are in red.

The ESI-MS spectrum of $[Rh_{10}Au(CO)_{26}]^{3}$ is reported in Figure 33, while its interpretation is reported in Table 1:

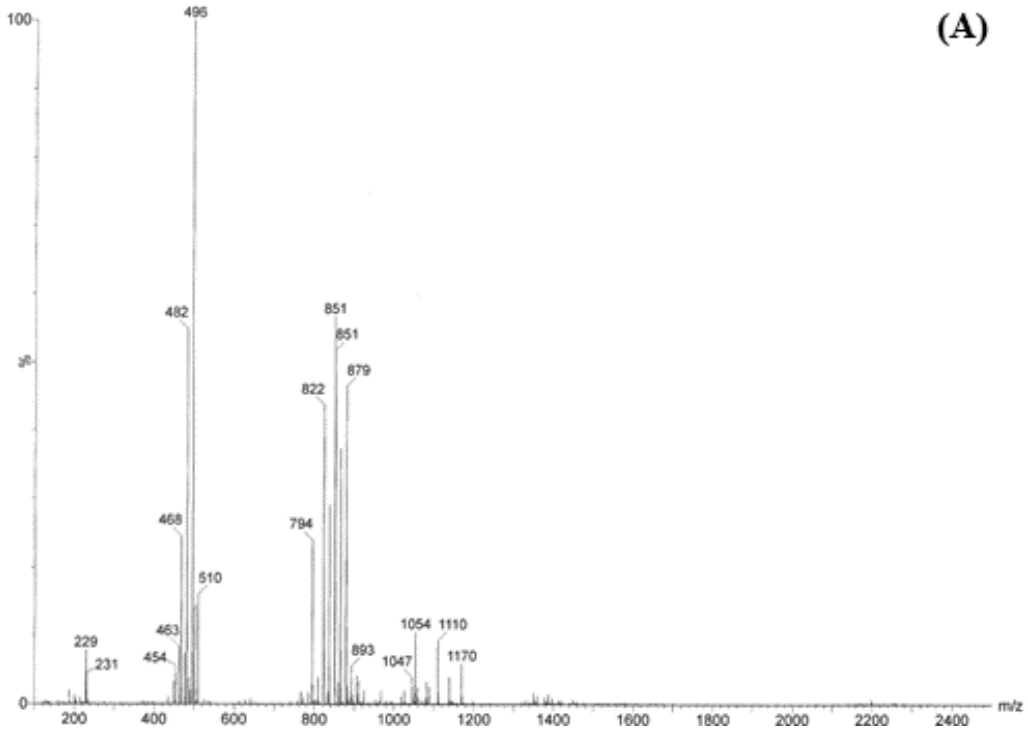

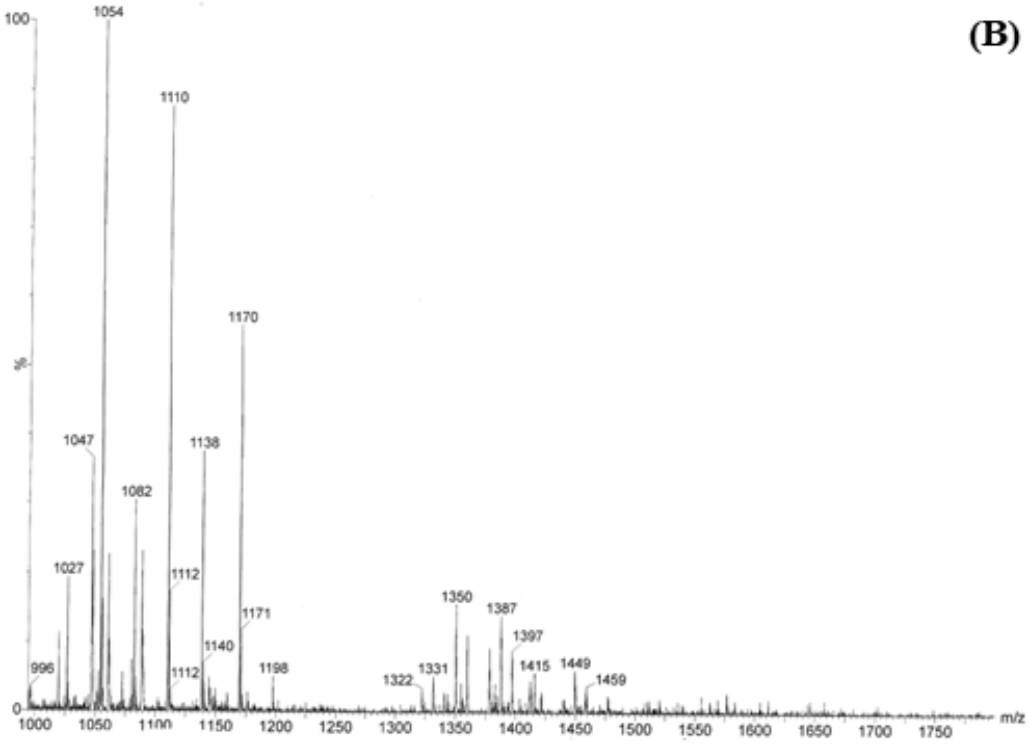
(B)
100
%
0
1054
1110
1170
1047
1138
1082
1027
1112
1171
1140
1350
1387
1397
996
1112
1198
1322
1331
1415
1449
1459
m/z
1000 1050 1100 1150 1200 1250 1300 1350 1400 1450 1500 1550 1600 1650 1700 1750

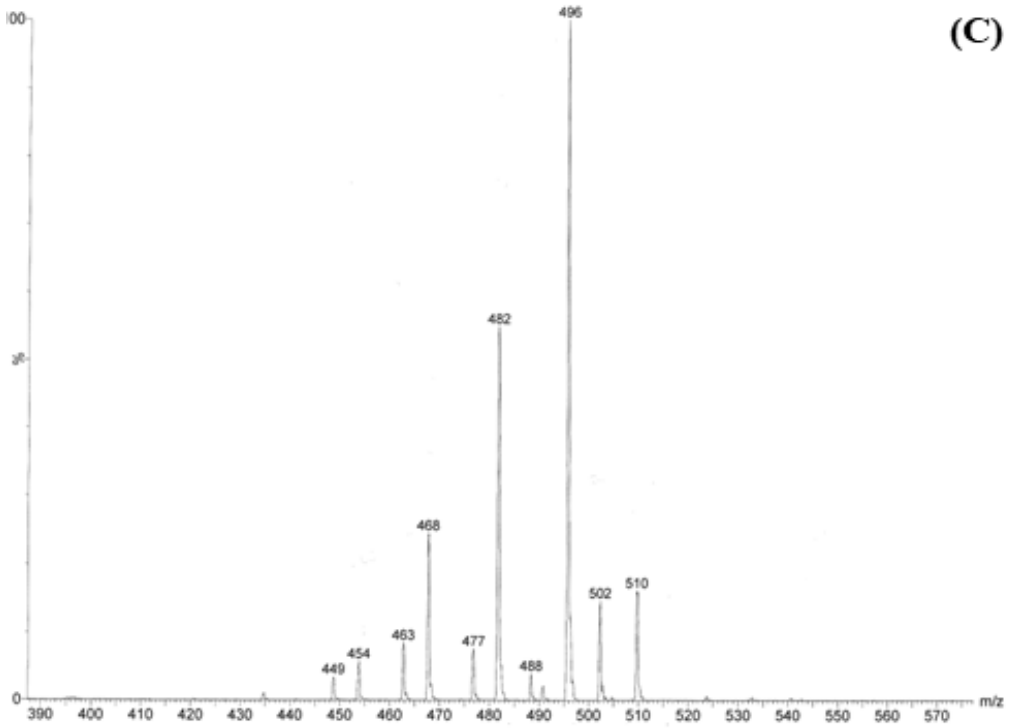
(C)
100
%
0
496
482
468
502
510
463
454
449
477
488
m/z
390 400 410 420 430 440 450 460 470 480 490 500 510 520 530 540 550 560 570

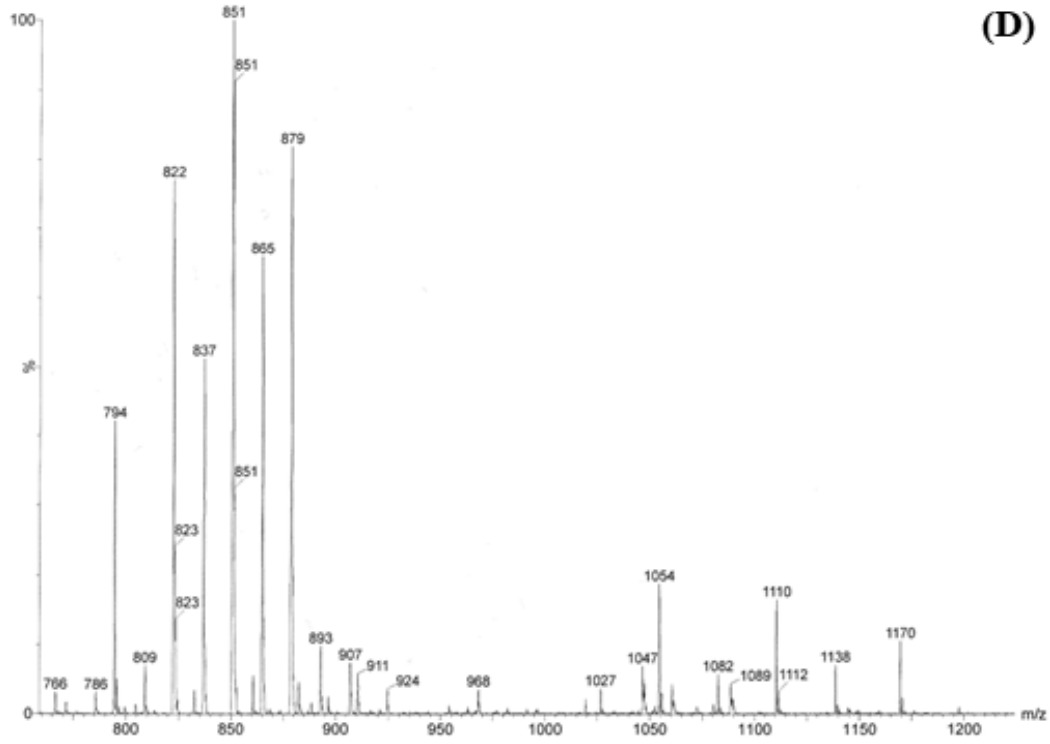

Figure 33: (A) ESI-MS spectrum of $[Rh_{10}Au(CO)_{26}][TMBA]_3$ crystals dissolved in CH_3CN, (B) augmentation 1, (C) augmentation 2 and (D) augmentation 3.

Signal (M/Z)	Molecular Ion
1198	*$[Rh_5Au(CO)_{12}][TMBA]$*
1170	*$[Rh_5Au(CO)_{11}][TMBA]$*
1047	$[Rh_5Au(CO)_{12}]^-$
893	*$[Rh_{10}Au(CO)_{20}]^{2-}$*
879	*$[Rh_{10}Au(CO)_{19}]^{2-}$*
865	*$[Rh_{10}Au(CO)_{18}]^{2-}$*
851	*$[Rh_{10}Au(CO)_{17}]^{2-}$*
837	*$[Rh_{10}Au(CO)_{16}]^{2-}$*
823	*$[Rh_{10}Au(CO)_{15}]^{2-}$*
809	*$[Rh_{10}Au(CO)_{14}]^{2-}$*

794	*$[Rh_{10}Au(CO)_{13}]^{2-}$*
510	$[Rh_5Au(CO)_{11}]^{2-}$
496	$[Rh_5Au(CO)_{10}]^{2-}$
482	$[Rh_5Au(CO)_9]^{2-}$
468	$[Rh_5Au(CO)_8]^{2-}$
454	$[Rh_5Au(CO)_7]^{2-}$

Table 1: Interpretation of the peaks of the ESI-MS spectrum of $[Rh_{10}Au(CO)_{26}][TMBA]_3$ crystals dissolved in CH_3CN.

The Au-Rh bond length varies between 2,881 Å and 2,968 Å and the Rh-Rh bond length varies between 2,712 Å and 2,788 Å.

	Average (Å)	Min (Å)	Max (Å)
Au-Rh	2,917 ± 0,044	2,881	2,968
Rh-Rh	2,740 ± 0,038	2,712	2,788

Table 2: Most significant bond lengths in $[Rh_{10}Au(CO)_{26}]^{3-}$.

Electronic counting reveals the cluster to be diamagnetic:

$$10Rh \times 9e^- + 1Au \times 11e^- + 26CO \times 2e^- + 3e^- = 156 \text{ CVE}$$

4.10 $[Rh_{16}Au_6(CO)_{36}]^{4-}$: molecular structure and spectroscopic characterization

The IR spectrum of the crystals dissolved in CH_3CN is reported in Figure 34.

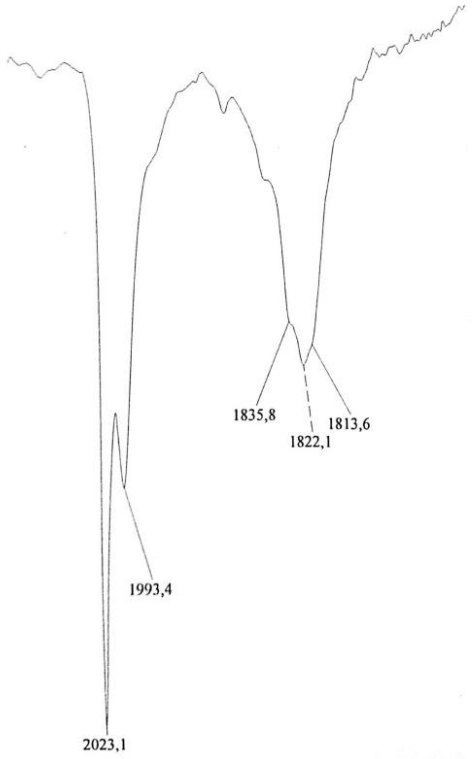

Figure 34: IR spectrum of $[Rh_{16}Au_6(CO)_{36}]^{4-}$ crystals dissolved in CH_3CN under CO atmosphere.

The spectrum displays a single intense peak at 2023vs cm^{-1}, along with a smaller peak at 1993m cm^{-1}, due to the stretching of terminal carbonyl ligands, and three peaks at 1835m, 1822m and 1814m cm^{-1} in the bridging carbonyl region.

The molecular structure of $[Rh_{16}Au_6(CO)_{36}]^{4-}$ (Figure 35) is composed by a central octahedron of gold atoms. Four Rh_4 fragments are present, each one capping two faces of the gold octahedron, creating two new Rh_4Au_2 octahedrons. A shell of thirty-six carbonyl ligands stabilizes the structure, sixteen of those in terminal position and twenty of those in double-bridging position.

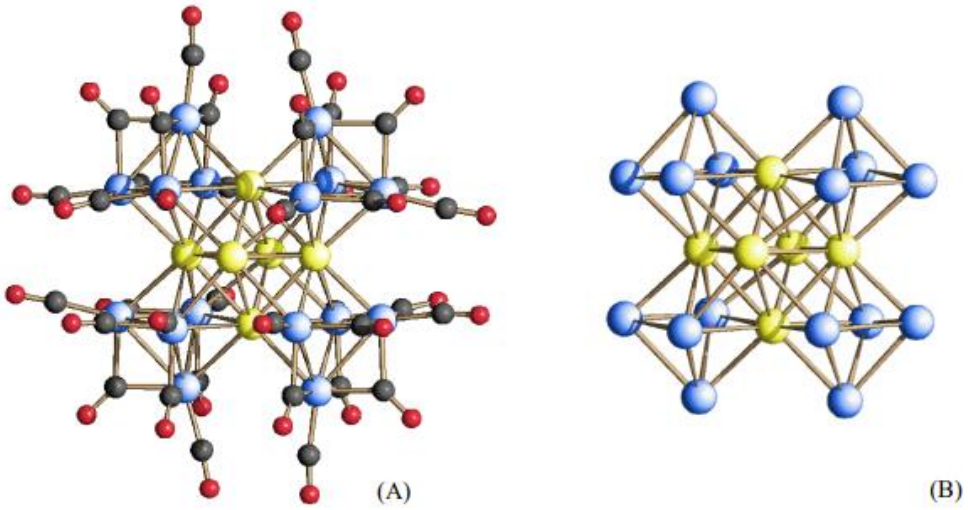

Figure 35: (A) Molecular structure of [$[Rh_{16}Au_6(CO)_{36}]^{4-}$ and (B) structure of the metallic backbone of $[Rh_{16}Au_6(CO)_{36}]^{4-}$. Rhodium atoms are represented in blue, carbon atoms are in grey, oxygen atoms are in red.

The ESI-MS spectrum of $[Rh_{16}Au_6(CO)_{36}]^{6-}$ is reported in Figure 36, while its interpretation is reported in Table 3:

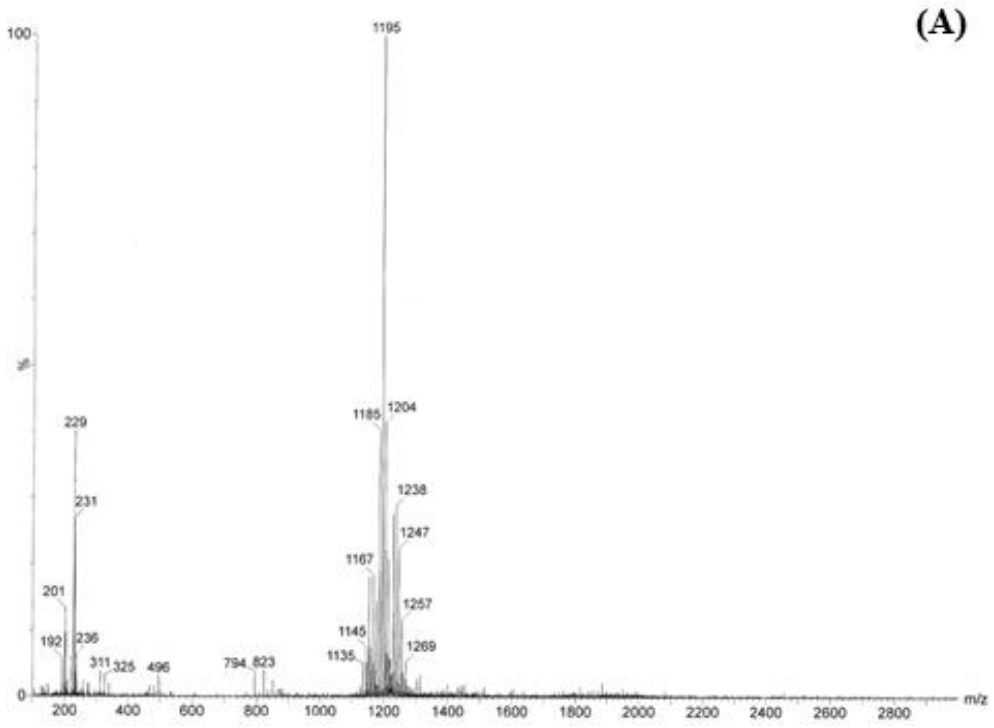

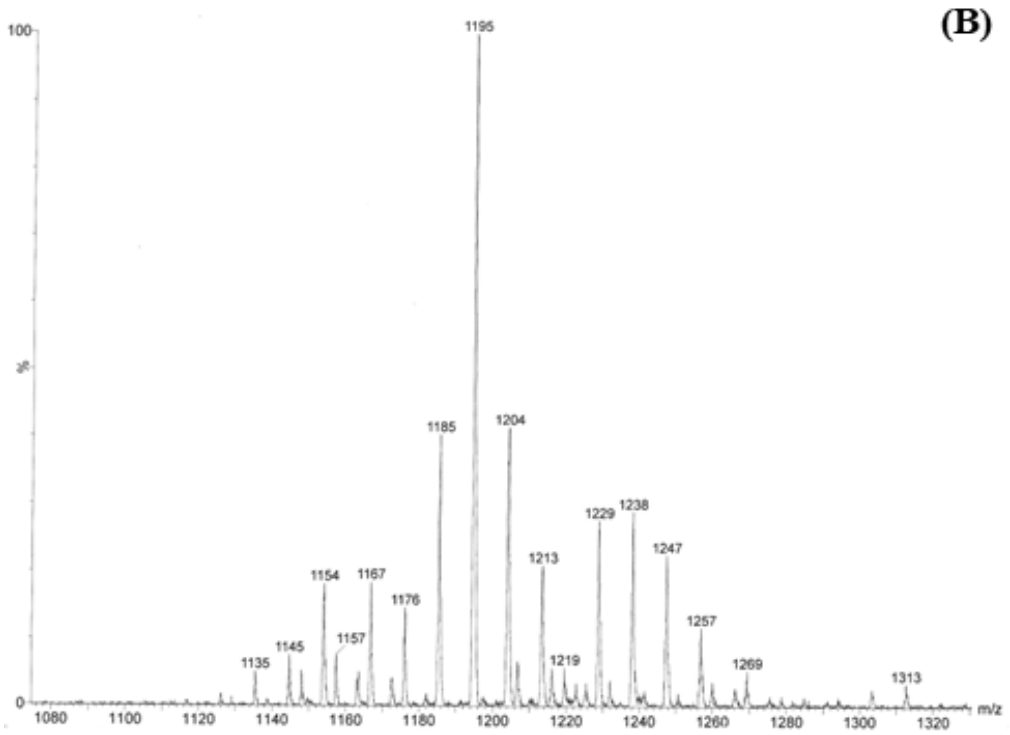

Figure 36: (A) ESI-MS spectrum of $[Rh_{16}Au_6(CO)_{36}][TMA]_4$ crystals dissolved in CH_3CN and (B) augmentation.

Signal (M/Z)	Molecular Ion
1257	*{[$Rh_{16}Au_6(CO)_{31}$][TMA]}$^{3-}$*
1247	*{[$Rh_{16}Au_6(CO)_{30}$][TMA]}$^{3-}$*
1238	*{[$Rh_{16}Au_6(CO)_{29}$][TMA]}$^{3-}$*
1229	*{[$Rh_{16}Au_6(CO)_{28}$][TMA]}$^{3-}$*
1219	*{[$Rh_{16}Au_6(CO)_{27}$][TMA]}$^{3-}$*
1213	$[Rh_{16}Au_6(CO)_{29}]^{3-}$
1204	$[Rh_{16}Au_6(CO)_{28}]^{3-}$
1195	$[Rh_{16}Au_6(CO)_{27}]^{3-}$
1185	$[Rh_{16}Au_6(CO)_{26}]^{3-}$

1176	$[Rh_{16}Au_6(CO)_{25}]^{3-}$
1167	$[Rh_{16}Au_6(CO)_{29}]^{3-}$

Table 3: Interpretation of the peaks of the ESI-MS spectrum of $[Rh_{16}Au_6(CO)_{36}][TMA]_4$ crystals dissolved in CH_3CN.

The Au-Au bond length varies between 2,605 Å and 2,829 Å, the Au-Rh bond length varies between 2,662 Å and 2,846 Å and the Rh-Rh bond length varies between 2,769 Å and 2,869 Å.

	Average (Å)	Min (Å)	Max (Å)
Au-Au	2,687 ± 0,112	2,605	2,829
Au-Rh	2,734 ± 0,092	2,662	2,846
Rh-Rh	2,829 ± 0,050	2,769	2,869

Table 4: Most significant bond lengths in $[Rh_{16}Au_6(CO)_{36}]^{4-}$.

Electronic counting reveals the cluster to be diamagnetic:

$$16Rh \times 9e^- + 6Au \times 11e^- + 36CO \times 2e^- + 4e^- = 286 \text{ CVE}$$

4.11 $[Rh_{16}Au_6(CO)_{36}]^{6-}$: molecular structure and spectroscopic characterization

The IR spectrum of the crystals dissolved in CH_3CN is reported in Figure 37:

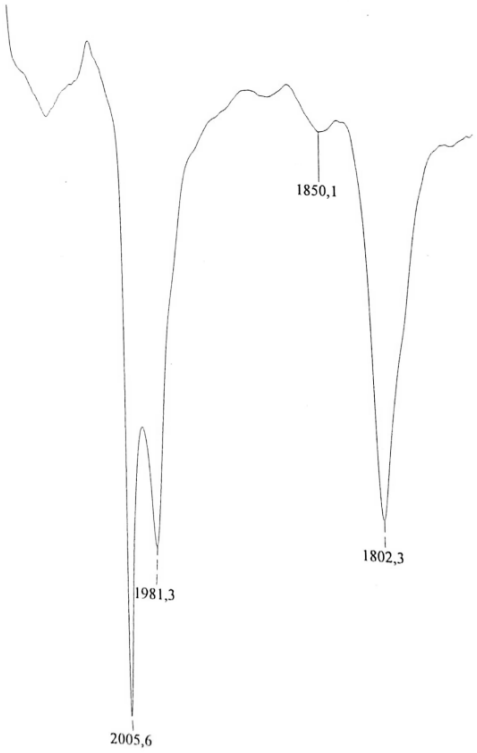

Figure 37: IR spectrum of $[Rh_{16}Au_6(CO)_{36}]^{6-}$ crystals dissolved in CH_3CN under CO atmosphere.

The spectrum displays a single high peak at 2005vs cm^{-1}, along with a smaller peak at 1981m cm^{-1}, due to the stretching of terminal carbonyl ligands, and a peak at 1802m cm^{-1} in the bridging carbonyl region.

The molecular structure of $[Rh_{16}Au_6(CO)_{36}]^{6-}$ (Figure 38) is composed by a central octahedron of gold atoms. Four Rh_4 fragments are present, each one capping two faces of the gold octahedron, creating two new Rh_4Au_2 octahedrons. A shell of thirty-six carbonyl ligands covers the structure, sixteen of those in terminal position and twenty of those in double-bridging position.

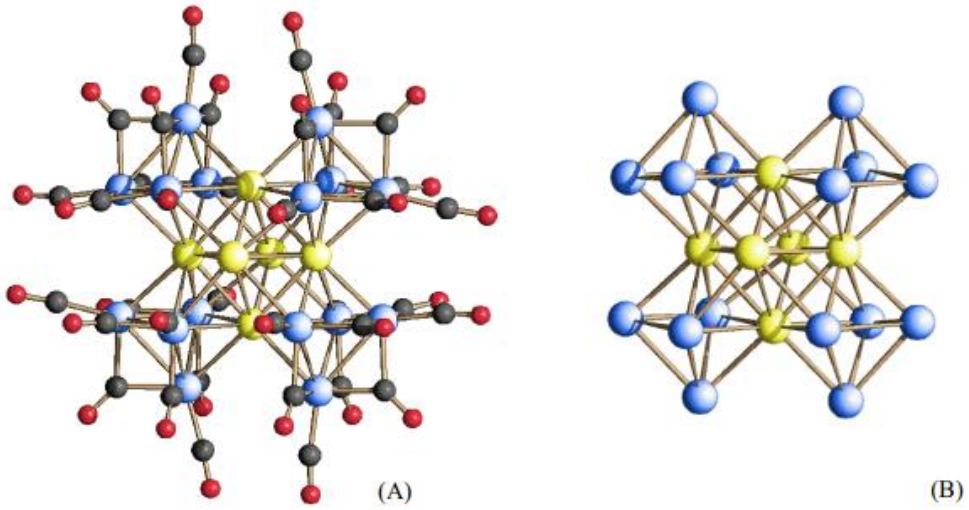

Figure 38: (A) Molecular structure of $[Rh_{16}Au_6(CO)_{36}]^{6-}$ and (B) structure of the metallic backbone of $[Rh_{16}Au_6(CO)_{36}]^{6-}$. Rhodium atoms are represented in blue, carbon atoms are in grey, oxygen atoms are in red.

The ESI-MS spectrum of $[Rh_{16}Au_6(CO)_{36}]^{6-}$ is reported in Figure 39, while its interpretation is reported in Table 5:

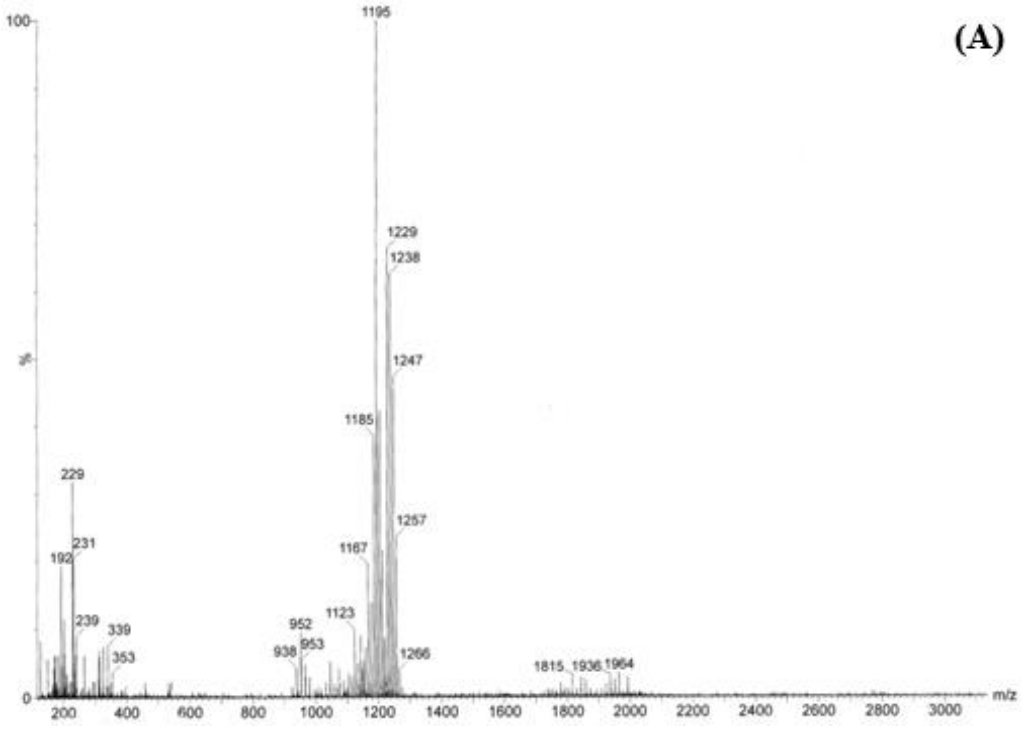

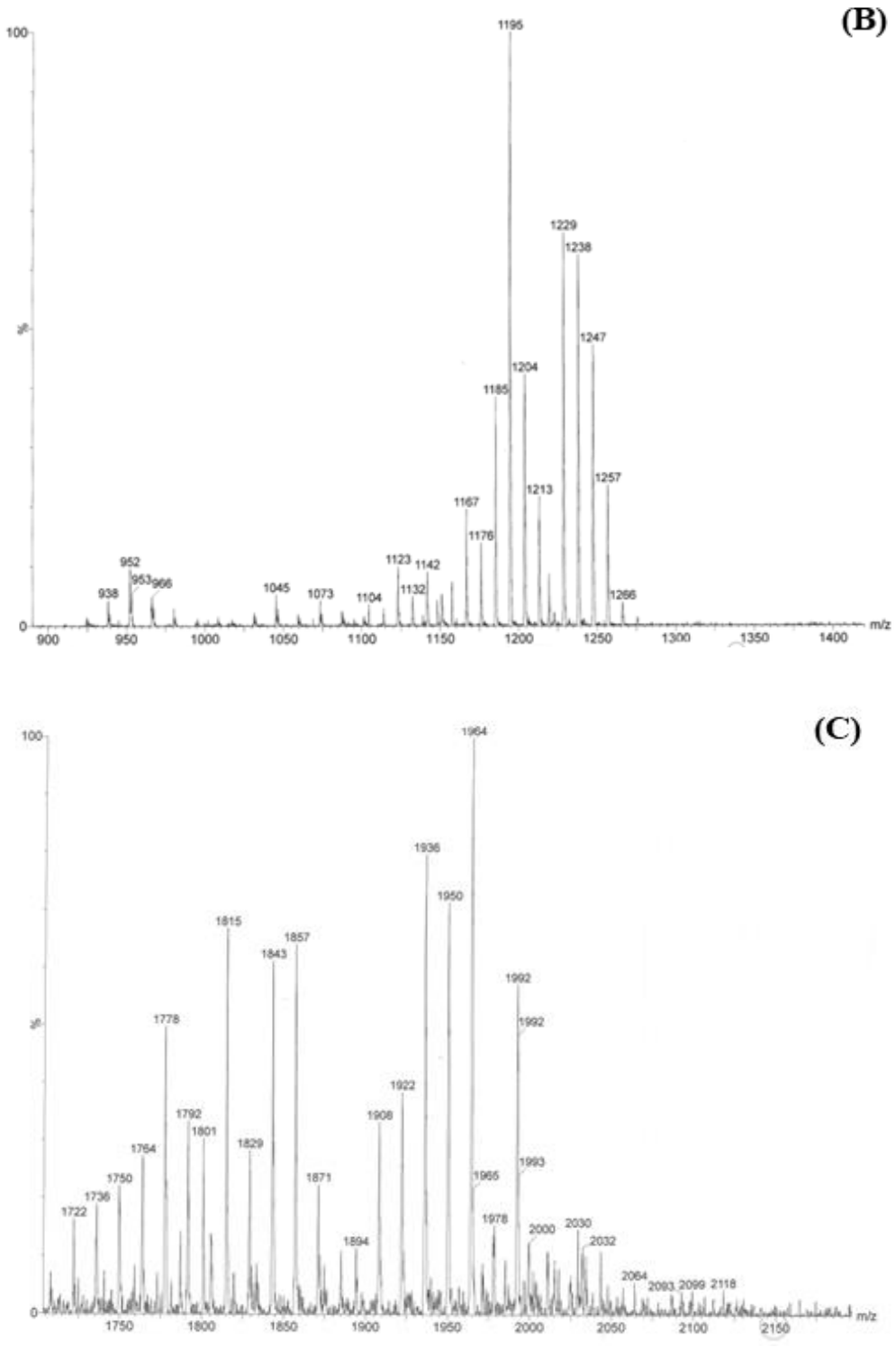

Figure 39: (A) ESI-MS spectrum of $[Rh_{16}Au_6(CO)_{36}][TEA]_6$ crystals dissolved in CH_3CN, (B) augmentation 1 and (C) augmentation 2.

Signal (M/Z)	Molecular Ion
1992	*$[Rh_{16}Au_6(CO)_{32}][TEA]_2$*
1978	*$[Rh_{16}Au_6(CO)_{31}][TEA]_2$*
1864	*$[Rh_{16}Au_6(CO)_{30}][TEA]_2$*
1950	*$[Rh_{16}Au_6(CO)_{29}][TEA]_2$*
1936	*$[Rh_{16}Au_6(CO)_{28}][TEA]_2$*
1922	*$[Rh_{16}Au_6(CO)_{27}][TEA]_2$*
1908	*$[Rh_{16}Au_6(CO)_{26}][TEA]_2$*
1894	*$[Rh_{16}Au_6(CO)_{25}][TEA]_2$*
1871	$[Rh_{16}Au_6(CO)_{28}][TEA]^-$
1857	$[Rh_{16}Au_6(CO)_{27}][TEA]^-$
1843	$[Rh_{16}Au_6(CO)_{26}][TEA]^-$
1829	$[Rh_{16}Au_6(CO)_{25}][TEA]^-$
1815	$[Rh_{16}Au_6(CO)_{24}][TEA]^-$
1801	$[Rh_{16}Au_6(CO)_{23}][TEA]^-$
1792	*$[Rh_{16}Au_6(CO)_{27}]^{2-}$*
1778	*$[Rh_{16}Au_6(CO)_{26}]^{2-}$*
1764	*$[Rh_{16}Au_6(CO)_{25}]^{2-}$*
1750	*$[Rh_{16}Au_6(CO)_{24}]^{2-}$*
1736	*$[Rh_{16}Au_6(CO)_{23}]^{2-}$*
1722	*$[Rh_{16}Au_6(CO)_{22}]^{2-}$*
1266	$\{[Rh_{16}Au_6(CO)_{30}][TEA]\}^{3-}$
1257	$\{[Rh_{16}Au_6(CO)_{29}][TEA]\}^{3-}$
1247	$\{[Rh_{16}Au_6(CO)_{28}][TEA]\}^{3-}$
1238	$\{[Rh_{16}Au_6(CO)_{27}][TEA]\}^{3-}$
1229	$\{[Rh_{16}Au_6(CO)_{26}][TEA]\}^{3-}$
1213	*$[Rh_{16}Au_6(CO)_{29}]^{3-}$*
1204	*$[Rh_{16}Au_6(CO)_{28}]^{3-}$*

1195	*$[Rh_{16}Au_6(CO)_{27}]^{3-}$*
1185	*$[Rh_{16}Au_6(CO)_{26}]^{3-}$*
1176	*$[Rh_{16}Au_6(CO)_{25}]^{3-}$*
1167	*$[Rh_{16}Au_6(CO)_{24}]^{3-}$*

Table 5: Interpretation of the peaks of the ESI-MS spectrum of $[Rh_{16}Au_6(CO)_{36}][TEA]_6$ crystals dissolved in CH_3CN.

The Au-Au bond length varies between 2,740 Å and 3,109 Å, the Au-Rh bond length varies between 2,712 Å and 2,890 Å and the Rh-Rh bond length varies between 2,809 Å and 2,861 Å. Bond lengths of $[Rh_{16}Au_6(CO)_{36}]^{4-}$ and $[Rh_{16}Au_6(CO)_{36}]^{6-}$ are quite different; as a matter of fact this is not an unusual phenomenon in multivalent clusters, where compounds with equal structures and same amount of carbonyl ligands happen to display longer bond lengths at higher negative charges.

	Average (Å)	Min (Å)	Max (Å)
Au-Au	2,885 ± 0,134	2,740	3,109
Au-Rh	2,797 ± 0,058	2,712	2,890
Rh-Rh	2,841 ± 0,019	2,809	2,861

Table 6: Most significant bond lengths in $[Rh_{16}Au_6(CO)_{36}]^{6-}$.

Electronic counting reveals the complex to be diamagnetic:

$$16Rh \times 9e^- + 6Au \times 11e^- + 36CO \times 2e^- + 6e^- = 288 \text{ CVE}$$

4.12 $[Rh_{19}Au_5(CO)_{40}]^{4-}$: molecular structure and spectroscopic characterization

The IR spectrum of the crystals dissolved in CH_3CN is reported in Figure 40.

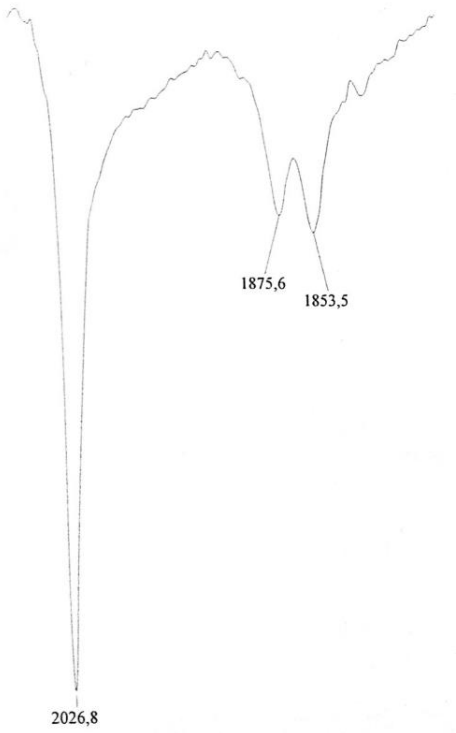

Figure 40: IR spectrum of $[Rh_{19}Au_5(CO)_{40}]^{4-}$ crystals dissolved in CH_3CN under CO atmosphere.

The spectrum displays a high peak in the terminal carbonyl zone at 2027vs cm^{-1}, and two peaks in the bridging carbonyl zone at 1875m and 1853m cm^{-1}.

The molecular structure of $[Rh_{19}Au_5(CO)_{40}]^{4-}$ (Figure 41) is composed by three prisms with a square base and a rectangular base, each one containing a gold atom in its centre. Each prism shares two vertices of the rectangular base with another prism. The metallic skeleton is completed by one rhodium and two gold atoms which connect the vertices of the prisms. A shell of forty carbonyl ligands covers the structure, sixteen of those in terminal position and twenty-four of those in double-bridging position.

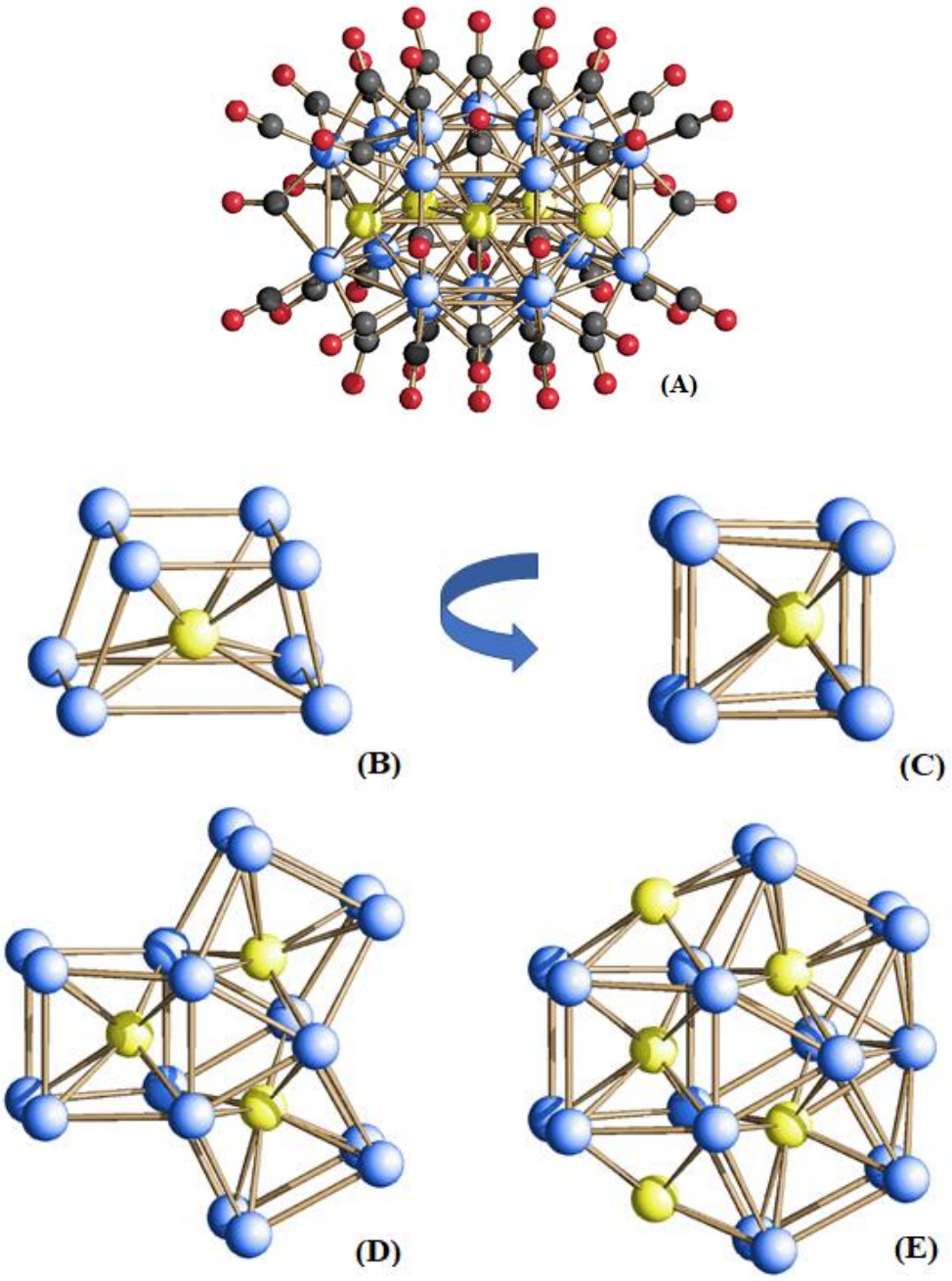

Figure 41: (A) Molecular structure of $[Rh_{19}Au_5(CO)_{40}]^{4-}$, (B) structure of a single prism unit, (C) prism unit rotated on the side, (D) structure created by the union of the three prism units and (E) structure of the whole metallic backbone of $[Rh_{19}Au_5(CO)_{40}]^{4-}$. Rhodium atoms are represented in blue, gold atoms are in yellow, carbon atoms are in grey, oxygen atoms are in red.

The Au-Au bond length varies between 2,905 Å and 3,027 Å, the Au-Rh bond length varies between 2,755 Å and 2,878 Å and the Rh-Rh bond length varies between 2,720 Å and 2,838 Å.

	Average (Å)	Min (Å)	Max (Å)
Au-Au	2,968 ± 0,061	2,905	3,027
Au-Rh	2,797 ± 0,062	2,755	2,878
Rh-Rh	2,805 ± 0,059	2,720	2,838

Table 7: Most significant bond lengths in $[Rh_{19}Au_5(CO)_{40}]^{4-}$.

Electronic counting reveals the complex to be diamagnetic:

$$19Rh \times 9e^- + 5Au \times 11e^- + 40CO \times 2e^- + 4e^- = 310 \text{ CVE}$$

4.13 $[Rh_{20}Au_7(CO)_{45}]^{5-}$: molecular structural and spectroscopic characterization

The IR spectrum of the crystal solution dissolved in CH_3CN is reported in Figure 42.

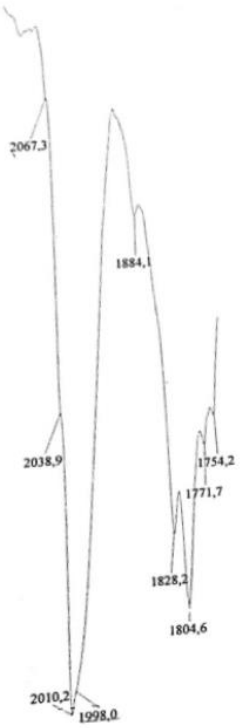

Figure 42: IR spectrum of solution which resulted in $[Rh_{20}Au_7(CO)_{45}]^{5-}$ crystal formation

The spectrum displays in the terminal carbonyl zone a high peak at 1989vs cm^{-1}, with shoulder-type peaks at 2010sh and 2032sh cm^{-1}, and a peak at 1824m cm^{-1} with shoulder-type peaks at 1803sh and 1765sh cm^{-1} in the bridging carbonyl zone.

The molecular structure of $[Rh_{20}Au_7(CO)_{45}]^{5-}$ (Figure 43) is composed by a central pentagon of gold atoms, capped on both faces by a gold atom. Five Rh_4 fragments are present, each one capping a side of the pentagon, creating five Rh_4Au_2 octahedrons. A shell of forty-five carbonyl ligands covers the structure, twenty of those in terminal position and twenty-five of those in double-bridging position.

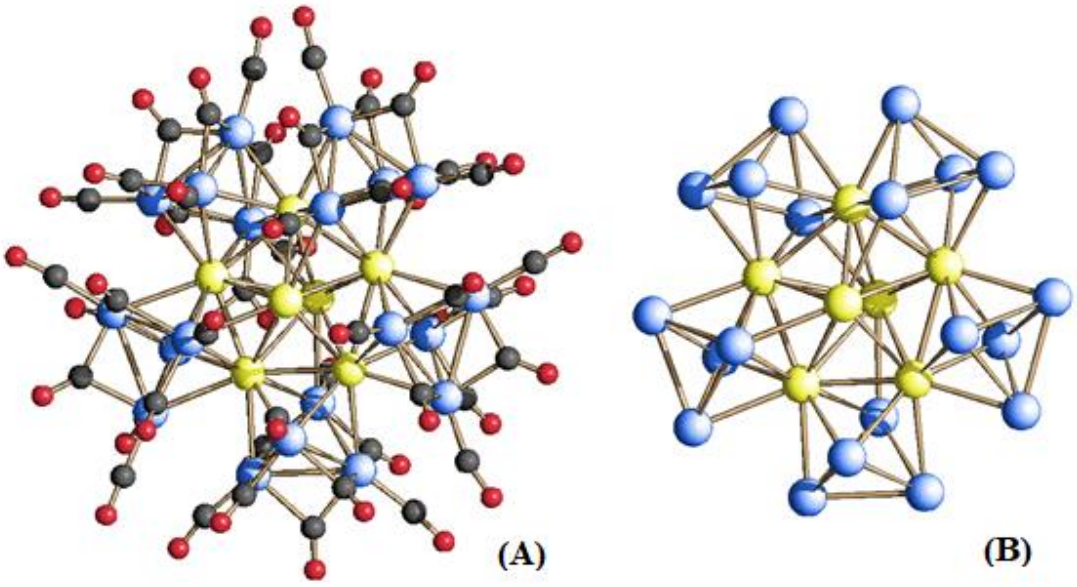

Figure 43: (A) Molecular structure of $[Rh_{20}Au_7(CO)_{45}]^{5-}$ and (B) structure of the metallic backbone of $[Rh_{20}Au_7(CO)_{45}]^{5-}$. Rhodium atoms are represented in blue, carbon atoms are in grey, oxygen atoms are in red

The Au-Au bond length varies between 2,743 Å and 3,035 Å, the Au-Rh bond length varies between 2,750 Å and 2,878 Å and the Rh-Rh bond length varies between 2,763 Å and 2,872 Å.

	Average (Å)	Min (Å)	Max (Å)
Au-Au	2,849 ± 0,146	2,743	3,035
Au-Rh	2,787 ± 0,064	2,750	2,878
Rh-Rh	2,821 ± 0,055	2,763	2,872

Table 8: Most significant bond lengths in $[Rh_{20}Au_7(CO)_{45}]^{5-}$.

Electronic counting reveals the complex to be diamagnetic:

$$20Rh \times 9e^- + 7Au \times 11e^- + 45CO \times 2e^- + 5e^- = 352 \text{ CVE}$$

5. CONCLUSIONS

This project was aimed at synthesizing and characterizing new high-nuclearity bimetallic clusters of rhodium and gold.

At the end of the project, new clusters have been synthesized: $[Rh_{10}Au(CO)_{26}]^{3-}$, $[Rh_{16}Au_6(CO)_{36}]^{4-}$, $[Rh_{19}Au_5(CO)_{40}]^{4-}$ and $[Rh_{20}Au_7(CO)_{45}]^{5-}$. They all have been characterized via FT-IR analysis, and single crystal X-ray diffractometry; the former two species have also been analysed via ESI-MS spectrometry. Moreover, a new synthetic pathway was discovered to synthetize $[Rh_{16}Au_6(CO)_{36}]^{6-}$. The former has been analysed via FT-IT analysis, single crystal X-ray diffractometry and ESI-MS spectrometry. Multiple synthetic pathways to obtain $[Rh_{10}Au(CO)_{26}]^{3-}$ were discovered, either by using Au(III) or Au(I) salts.

The reactivity of $[Rh_{10}Au(CO)_{26}]^{3-}$ was studied, both via oxidation with $[AuCl_4]^-$ and acidification, proving that the formation of the $[Rh_{16}Au_6(CO)_{36}]^{4-}$ cluster follows a consecutive reaction pathway starting from $[Rh_{10}Au(CO)_{26}]^{3-}$.

Overall, it is possible to summarize the results as follow:

- The IR spectra at the end of every reaction are rather similar, despite some minor differences; in fact, no matter what gold oxidizing agent is employed, the reaction seem to lead towards the formation of a mixture of bimetallic ($[Rh_{10}Au(CO)_{26}]^{3-}$, $[Rh_{16}Au_6(CO)_{36}]^{4-}$, $[Rh_{16}Au_6(CO)_{36}]^{6-}$, $[Rh_{19}Au_5(CO)_{40}]^{4-}$, $[Rh_{20}Au_7(CO)_{45}]^{5-}$) and homometallic Rh clusters ($[Rh(CO)_2Cl_2]^-$, $[Rh_5(CO)_{15}]^-$). The concentration of each is mostly affected by the Rh:Au stoichiometric ratio, while the crystallization is influenced by packing effects involving the cluster counterion and employed solvent.

- Au(I) reactions in CH_3CN lead towards the obtainment of $[Rh_{10}Au(CO)_{26}]^{3-}$ at lower Rh:Au ratios (1:2.5 – 1:6), while it was possible to synthetise and

crystallize a by-product ($[Rh_{20}Au_7(CO)_{45}]^{5-}$ as TMBA salt) at a higher ratio (1:2.25).

- The reactivity in DMF leads towards the formation of $[Rh_{10}Au(CO)_{26}]^{3-}$ at high Rh:Au ratios (1:1 for Au(III), 1:3 for Au(I)), while at lower ratios the reactions proceed towards the formation of $[Rh_{16}Au_6(CO)_{36}]^{4-}$, which was found to follow a consecutive reaction pathway starting from $[Rh_{10}Au(CO)_{26}]^{3-}$.

- Similarly, the reactivity in THF leads towards the formation of $[Rh_{10}Au(CO)_{26}]^{3-}$ at higher Rh:Au ratios (1:0,5) and of $[Rh_{16}Au_6(CO)_{36}]^{6-}$ at lower ratios (1:1).

- Au(III) reactivity in acetone leads towards the formation of $[Rh_{19}Au_5(CO)_{40}]^{4-}$ at a Rh:Au ratio of 1:1. The cluster crystallized with a mixed combination of TEA^+ and TPA^+ counterions.

A summary of all the reaction products is reported in Table 6. Crystal formation of species has been explicitly stated if occurred.

Reagent N°1	Reagent N°2	S.R.	Cation	Solvent	EtOH	CH_2Cl_2	THF	Acetone
$[Rh_7(CO)_{16}][TMBA]_3$	$[AuCl_4][TMBA]$	1:1	$TMBA^+$	DMF	$[Rh_5(CO)_{15}]^-$	-	$[Rh_5(CO)_{15}]^-$	Crystals of $[Rh_{10}Au(CO)_{26}][TMBA]_3$
$[Rh_7(CO)_{16}][TMBA]_3$	$[AuCl_4][TMBA]$	1:2	$TMBA^+$	DMF	$[Rh(CO)_2Cl_2]^-$ $[Rh_5(CO)_{15}]^-$	-	$[Rh_5(CO)_{15}]^-$	Crystals of $[Rh_{16}Au_6(CO)_{36}][TMBA]_4$
$[Rh_7(CO)_{16}][TEA]_3$	$[AuCl_4][TEA]$	1:2	TEA^+	DMF	$[Rh(CO)_2Cl_2]^-$ $[Rh_5(CO)_{15}]^-$	-	$[Rh_5(CO)_{15}]^-$	Crystals of $[Rh_{16}Au_6(CO)_{36}][TMA]_4$
$[Rh_7(CO)_{16}][TBA]_3$	$[AuCl_4][TEA]$	1:1	TBA^+ TEA^+	THF	Solution: $[Rh(CO)_2Cl_2]^-$ $[Rh_5(CO)_{15}]^-$	Solution: $[Rh_{10}Au(CO)_{26}]^{3-}$	-	Precipitate: Crystals of $[Rh_{16}Au_6(CO)_{36}][TEA]_6$
$[Rh_7(CO)_{16}][TBA]_3$	$[AuCl_4][TEA]$	1:0,5	TBA^+ TEA^+	THF	Solution: $[Rh(CO)_2Cl_2]^-$ $[Rh_5(CO)_{15}]^-$	Solution: $[Rh_{10}Au(CO)_{26}]^{3-}$	Solution: $[Rh_{10}Au(CO)_{26}]^{3-}$	Precipitate: $[Rh_{10}Au(CO)_{26}]^{3-}$
$[Rh_7(CO)_{16}][TPA]_3$	$[AuCl_4][TEA]$	1:1	TPA^+ TEA^+	Acetone	$[Rh(CO)_2Cl_2]^-$	Extremely diluted and mixed spectum	$[Rh_5(CO)_{15}]^-$	Crystals of $[Rh_{12}(CO)_{30}]^{2-}$ and $[Rh_{19}Au_5(CO)_{40}]$ $[TEA]_2[TPA]_2$

Reagent N°1	Reagent N°2	S.R.	Cation	Solvent	EtOH	CH_2Cl_2	THF	Acetone
$[Rh_7(CO)_{16}][TEA]_3$	$Au(Et_2S)Cl$	1:2,25	TEA^+	CH_3CN	$[Rh(CO)_2Cl_2]^-$ $[Rh_5(CO)_{15}]^-$	-	$[Rh_5(CO)_{15}]^-$	Crystals of $[Rh_{20}Au_7(CO)_{45}][TEA]_5$.
$[Rh_7(CO)_{16}][TMBA]_3$	$Au(Et_2S)Cl$	1:2,5	$TMBA^+$	CH_3CN	$[Rh(CO)_2Cl_2]^-$ $[Rh_5(CO)_{15}]^-$	-	Crystals of $[Rh_{10}Au(CO)_{26}][TMBA]_3$	Crystals of $[Rh_{10}Au(CO)_{26}][TMBA]_3$
$[Rh_7(CO)_{16}][TMBA]_3$	$Au(Et_2S)Cl$	1:6	$TMBA^+$	CH_3CN	$[Rh(CO)_2Cl_2]^-$ $[Rh_5(CO)_{15}]^-$	-	Crystals of $[Rh_{10}Au(CO)_{26}][TMBA]_3$	Crystals of $[Rh_{10}Au(CO)_{26}][TMBA]_3$
$[Rh_7(CO)_{16}][TMBA]_3$	$Au(Et_2S)Cl$	1:3	$TMBA^+$	DMF	$[Rh_5(CO)_{15}]^-$	-	$[Rh_5(CO)_{15}]^-$	Crystals of $[Rh_{10}Au(CO)_{26}][TMBA]_3$

Reactivity of $[Rh_{10}Au(CO)_{26}]^{3-}$

- $[Rh_{10}Au(CO)_{26}]^{3-}$ + $[AuCl_4][TMBA]$ in DMF: the reaction results in $[Rh_{16}Au_6(CO)_{36}]^{4+}$ formation.
- $[Rh_{10}Au(CO)_{26}]^{3-}$ + HBF_4 in CH_2Cl_2: : the reaction results in $[Rh_{16}Au_6(CO)_{36}]^{4+}$ formation.

Table 9: Summary of the reactions' results.

6. EXPERIMENTAL

Due to the intrinsic instability of these cluster to air exposure, in order to avoid their decomposition, all of the reactions were run applying the Schlenk technique under controlled CO atmosphere.

All the solvents that were used in the synthetic pathways were degassed before use and kept under N_2 atmosphere. THF was anhydrified applying a distillation process with sodium benzophenone.

The IR spectra were by an FT-IR Perkin Elmer SpectrumOne interferometer with 4 cm^{-1} resolution, employing CaF_2 cells of 1 mm thickness.

The ESI-MS analyses were run by the instrument Waters Micromass ZQ 4000.

The crystalline structures were characterized by single crystal X-ray diffractometry Bruker APEX II with CMOS area detector and Mo-Kα source.

6.1 $Rh_4(CO)_{12}$ synthesis

$$RhCl_3 + 2Cu + 2CO + Cl^- \rightarrow [Rh(CO)_2Cl_2]^- + 2CuCl$$

$$4[Rh(CO)_2Cl_2]^- + 6CO + 2H_2O \rightarrow \mathbf{Rh_4(CO)_{12}} + 2CO_2 + 4Cl^- + 4HCl$$

1 dm^3 of H_2O is added in a 2 dm^3 balloon. The system is degassed, then 5 g of $RhCl_3 \cdot nH_2O$ e 4,0 g di NaCl are added under continuous CO flux and vigorous stirring. 4,2 g of powdered Cu are added, and the reaction begins; the colour of the solution drifts from brick-red to colourless, while an orange suspension develops. After 8h, 10 cm^3 of a sodium citrate 1 M solution are added, in order to create a buffer system at pH 4. After 12 h, the reaction is considered as complete. The orange solid is filtered and washed with H_2O, then dried *in vacuo* and extracted in CH_2Cl_2. The final product is stored in solid state under CO atmosphere. $Rh_4(CO)_{12}$ appears as an orange powder. The overall yield for the synthetic pathway ranges between 86% and 99%.

6.2 $[Rh_7(CO)_{16}]^{3-}$ synthesis

$$7Rh_4(CO)_{12} + 12OH^- \rightarrow 4\mathbf{[Rh_7(CO)_{16}]^{3-}} + 14CO + 6CO_2 + 6H_2O$$

The reaction is run under a highly alkaline conditions, so as to avoid the formation of the $[Rh_6(CO)_{15}]^{2-}$ cluster, unstable in basic environments.

20 cm^3 of MeOH and solid $Rh_4(CO)_{12}$ are added into a CO-saturated schlenk. Then, KOH is added in a OH^-:Rh_4 stoichiometric ratio of 30:1, under vigorous stirring. After 24 h, the solution is filtered and the desired cation (TEA^+, TMA^+, $TMBA^+$, TBA^+), dissolved in H_2O, is added through a metathesis reaction. The solution is filtered one more time and dried *in vacuo*. The final product is stored in solid state under CO atmosphere. $[Rh_7(CO)_{16}]^{3-}$ salts appear as a fine green powder.

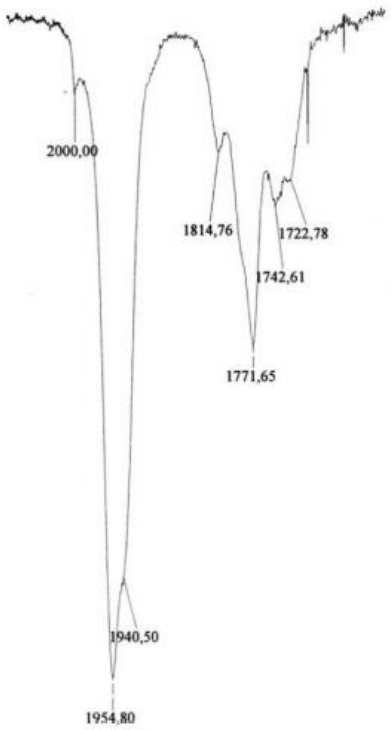

Figure 44: IR spectrum of $[Rh_7(CO)_{16}][TEA]_3$ crystals dissolved in CH_3CN.

6.3 $[Rh_{10}Au(CO)_{26}][TMBA]_3$ synthesis

A solution of $[AuCl_4][TMBA]$ in DMF is added dropwise, under controlled CO atmosphere, to a solution of $[Rh_7(CO)_{16}][TMBA]_3$ in DMF until a $Rh_7:Au^{3+}$ stoichiometric ration of 1:1 is reached. The reaction is allowed to react up to 24-48h and, once the IR spectrum displays the peaks of interest (1982s, 2008m, 2026m, 1825m cm^{-1}), the solution is reacted through a metathesis reaction with a solution of TMBACl in H_2O. The solid precipitate is washed with H_2O, then low-nuclearity by-products are solubilized through extractions in EtOH and THF. The cluster of interest $[Rh_{10}Au(CO)_{26}]^{3-}$ is extracted in acetone. Crystals are obtained by layering. The IR spectrum resulted from dissolving a few crystals in CH_3CN is reported in Figure 45.

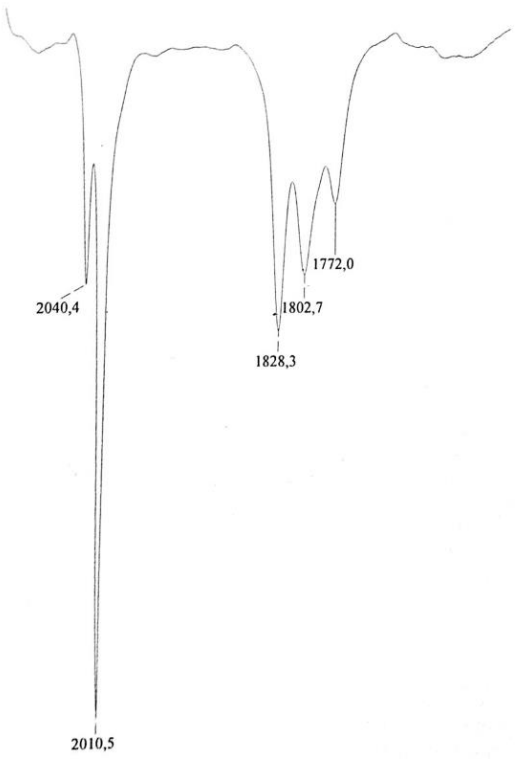

Figure 45: IR spectrum of $[Rh_{10}Au(CO)_{26}][TMBA]_3$ crystals dissolved in CH_3CN.

6.4 $[Rh_{16}Au_6(CO)_{36}][TMA]_4$ synthesis

A solution of $[AuCl_4][TEA]$ in DMF is added dropwise, under controlled CO atmosphere, to a solution of $[Rh_7(CO)_{16}][TEA]_3$ in DMF until a $Rh_7:Au^{3+}$ stoichiometric ration of 1:2 is reached. The reaction is allowed to react up to 24-48h and, once the IR spectrum displays the peaks of interest (2062s, 1983vs, 1824m, 1817m cm^{-1}), the solution is reacted through a metathesis reaction with a solution of TMACl in H_2O. The solid precipitate is washed with H_2O, then low-nuclearity by-products are solubilized through extractions in EtOH and THF. The cluster of interest $[Rh_{16}Au_6(CO)_{36}]^{4-}$ is extracted in acetone. Crystals are obtained by layering The IR spectrum resulted from dissolving a few crystals in CH_3CN is reported in Figure 46.

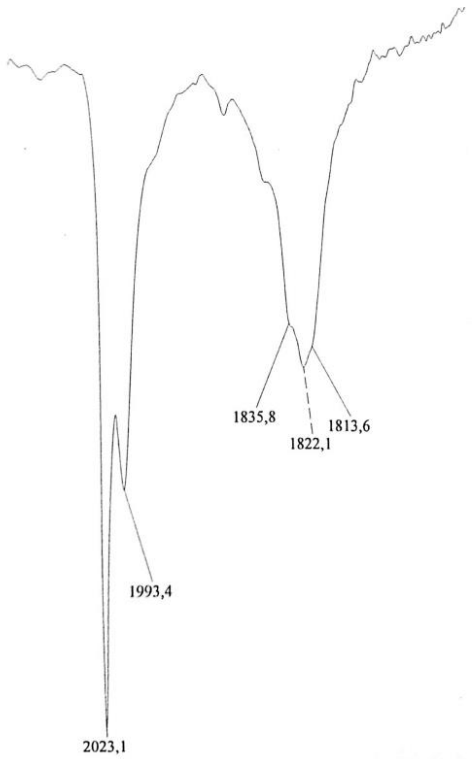

Figure 46: IR spectrum of $[Rh_{16}Au_6(CO)_{36}][TMA]_4$ crystals dissolved in CH_3CN.

6.5 $[Rh_{16}Au_6(CO)_{36}][TEA]_6$ synthesis

A solution of $[AuCl_4][TEA]$ in THF is added dropwise, under controlled CO atmosphere, to a solution of $[Rh_7(CO)_{16}][TBA]_3$ in THF until a Rh^7:Au^{3+} stoichiometric ration of 1:1 is reached. The reaction is allowed to react up to 24-48h and, once the IR spectrum displays the peaks of interest (2026sh, 2008sh, 1827m, 1807sh, 1771sh cm^{-1}), the naturally occurring solid precipitate is collected and dried. The solid precipitate is washed with H_2O, then the cluster of interest $[Rh_{16}Au_6(CO)_{36}]^{6-}$ is extracted in acetone. Crystals are obtained by layering The IR spectrum resulted from dissolving a few crystals in CH_3CN is reported in Figure 47.

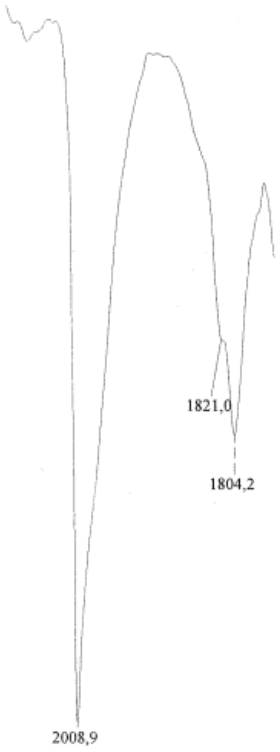

Figure 47: IR spectrum of $[Rh_{16}Au_6(CO)_{36}]^{6-}$ crystals dissolved in CH_3CN.

6.6 $[Rh_{19}Au_5(CO)_{40}][TEA]_2[TPA]_2$ synthesis

A solution of $[AuCl_4][TEA]$ in acetone is added dropwise, under controlled CO atmosphere, to a solution of $[Rh_7(CO)_{16}][TPA]_3$ in acetone until a $Rh_7:Au^{3+}$ stoichiometric ration of 1:1 is reached. The reaction is allowed to react up to 24-48h and, once the IR spectrum displays the peaks of interest (1984s, 2008sh, 2026sh, 1826m cm^{-1}), then the solution is dried *in vacuo*. The solid obtained is washed with H_2O, then low-nuclearity by-products are solubilized through extractions in EtOH and THF. The cluster of interest $[Rh_{19}Au_5(CO)_{40}]^{4-}$ is extracted in acetone. Crystals are obtained by layering. The IR spectrum resulted from dissolving a few crystals in CH_3CN is reported in Figure 48.

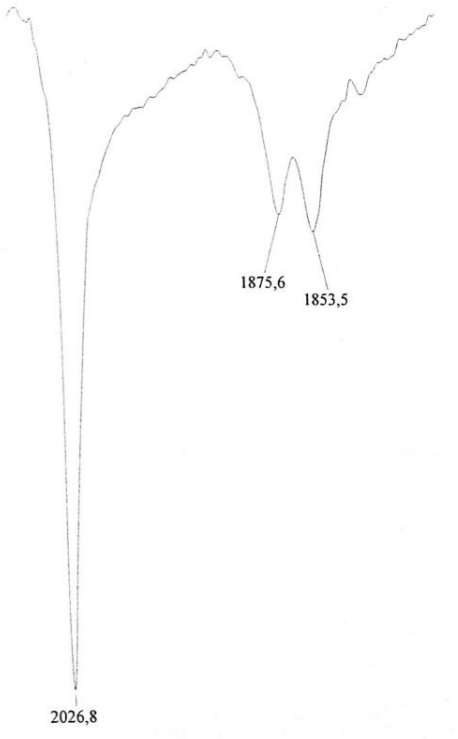

Figure 48: IR spectrum of $[Rh_{19}Au_5(CO)_{40}][TEA]_2[TPA]_2$ crystals dissolved in CH_3CN.

6.7 $[Rh_{20}Au_7(CO)_{45}][TEA]_5$ synthesis

A solution of $Au(Et_2S)Cl$ in CH_3CN is added dropwise, under controlled CO atmosphere, to a solution of $[Rh_7(CO)_{16}][TEA]_3$ in CH_3CN until a $Rh_7:Au^+$ stoichiometric ration of 1:2,25 is reached. The reaction is allowed to react up to 24-48h and, once the IR spectrum displays the peaks of interest (1989vs, 2010sh, 2032sh, 1824m, 1803sh, 1765sh cm^{-1}), then the solution is dried *in vacuo*. The solid obtained is washed with H_2O, then low-nuclearity by-products are solubilized through extractions in EtOH and THF. The cluster of interest $[Rh_{20}Au_7(CO)_{45}]^{5-}$ is extracted in acetone. Crystals are obtained by layering. The IR spectrum over the crystal solution is reported in Figure 49.

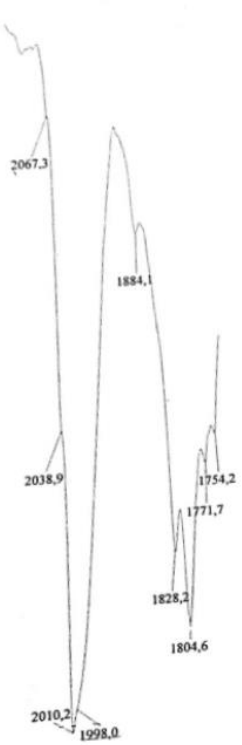

Figure 49: IR spectrum of the CH_3CN solution which resulted in $[Rh_{20}Au_7(CO)_{45}][TEA]_5$ crystals formation.

References

[1] F. A. Cotton, *Quarterly Review, Chemical Society*, **1966**, *416*.

[2] I. Ciabatti, "*Dalla scoperta del nichel tetracarbonile alla sintesi di nanocondensatori molecolari ad elevata nuclearità*", Rendiconti Accademia Nazionale delle Scienze detta dei XL, Memorie di Scienze Chimiche Naturali **2014**, 45-57.

[3] D. M. P. Mingos, *Pure & Applied Chemistry***, 1991**, *Vol. 63*, No. 6, 807-812.

[4] J. W. Lauher, *American Chemical Society*. **1978**, 5305-5315.

[5] G. Longoni, C. Femoni, M. C. Iapalucci, P. Zanello, *Metal Clusters in Chemistry*, P. Braunstein, L. A. Oro, P. R. Raithby Eds., Wiley-VCH, **1999**, *Vol. 2*, 1137-1158.

[6] S. Zacchini, *European Journal of Inorganic Chemistry,* **2011**, 4126-4129.

[7] P. Chini, *Journal of Organometallic Chemistry*, **1980**, *200*, 37.

[8] P. Chini, S. Martinengo, G. Giordano, *Gazzetta Chimica Italiana*, **1972**, *102*, 330-333.

[9] K. Wade, *Inorganic and Nuclear Chemistry Letters*, **1978**, *14*, 71-74.

[10] D. S. Dolzhnikov, M.C. Iapalucci, G. Longoni, C. Tiozzo, S. Zacchini, C. Femoni, *Journal of Inorganic Chemistry*, **2012**, *51*, 11214-11216.

[11] I. O. Koshevoy, M. Haukka, T. A. Pakkanen, S. P. Tunik, P. Vainiotalo, *Organometallics,* **2005**, *24*, 3516-3526.

[12] A. Fumagalli, S. Martinengo, G. Bernasconi, G. Ciani, D.M. Proserpio, A. Sironi, J., *American Chemical Society*, **1997**, *119*, 1450-1451.

[13] J. L. Vidal, W. E. Walker, R. L. Pruett, R.C. Schoening, *Inorganic Chemistry*, **1979**, *Vol. 18*, No. 1, 129-136.

[14] J. L. Vidal, W. E. Walker, R. C. Schoening, *Inorganic Chemistry*, **1981**, *20*, 238-242.

[15] J. L. Vidal, R.A. Fiato, L. A. Cosby, R. L. Pruett, *Inorganic Chemistry*, **1978**, *Vol. 17*, No. 9, 2574-258

[16] J. L. Vidal, *Inorganic Chemistry*, **1981**, *20*, 243-249.

[17] C. Femoni, M. C. Iapalucci, G. Longoni, C. Tiozzo, S. Zacchini, B. T. Heaton, J. A. Iggo, *Dalton Trans*. **2007**, *35*, 3914-3923.

[18] J. L. Vidal, J. M. Troup, *Journal of Organometallic Chemistry*, **1981**, *213*, 351.

[19] C. Femoni, I. Ciabatti, M. C. Iapalucci, S. Ruggieri, S. Zacchini, *Progress In Natural Science: Materials International*, **2016**, *26*, 461-466.

[20] S. Ruggieri, *Master's Degree Thesis*, **2015**.

[21] C. Femoni, G. Bussoli, I. Ciabatti, M. Ermini, M. Hayatifar, M. C. Iapalucci, S. Ruggieri, S. Zacchini, *Inorganic Chemistry*, **2017**, *56*, 6343-6351.

[22] R. D. Adams, J. L. Smith Jr, *Inorganic Chemistry*, **2005**, *44*, 4276.

[23] A. Boccalini, *Bachelor's Degree Thesis*, **2016**.

[24] A. Fumagalli, S. Martinengo, G. Ciani, N. Masciocchi, A. Sironi, *Inorganic Chemistry*, **1992**, *31*, 336-340

[25] I. Ciabatti, C. Femoni, M.C. Iapalucci, S. Ruggieri, S. Zacchini, *Coordination Chemistry Reviews*, **2018**, *355*, 27-38.

[26] H. Schmidbaur, Gold. Bull. 23 (1990) 11-21.

[27] H. Schmidbaur, A. Schier, Chemical. Society Reviews 37 (2008) 1931-1951.

[28] J. Alison, J. Whoolery, S. Brock, F. Lawrence, *Inorganic Chemistry,* **1994**, *227*, 269-283.

[29] I. Ciabatti, C. Femoni, M.C. Iapalucci, G. Longoni, S. Zacchini, S. Fedi, F. Fabrizi de Biani, *Inorganic Chemistry,* **2012**, *51*, 11753-11761.

[30] Angelici and Robert J., *Inorganic Syntheses Volume 28 || Tri-μ-Carbonyl-Nonacarbonyltetra-Rhodium, Rh4(CO)9(μ-CO)3,* **1990**, 242–245.

[31] Albano, Vincenzo G.; Bellon, Pier L.; Ciani, Gianfranco, *Crystal and molecular structure of the anion [Rh7(CO)16]3- in its tetramethylammonium salt*, ***1988***, Journal of the Chemical Society, Dalton Transactions, (*4*), 110

[32] G. Bussoli, *Master's Degree Thesis*, **2017**.